Nearby stars of the Galactic disk and halo [*]

Klaus Fuhrmann

Institut für Astronomie und Astrophysik der Universität München, Scheinerstraße 1, 81679 München, Germany

Abstract. Model atmosphere analyses of échelle spectra of some fifty nearby F- and G-type stars are presented. The sample is confined to the main-sequence, turnoff and subgiant region, regardless of the metal abundance. On the base of these data, spectroscopic parallaxes are calculated and compared to the Hipparcos astrometry to explore the reliability of the derived stellar parameters, notably the surface gravity and metal abundance scale.

The spectroscopic distance scale is found in good agreement with the Hipparcos parallaxes and is characterized by a 5% *rms* uncertainty. The results suggest a precision in $\log g$ of ~ 0.1 dex, and $0.05 - 0.10$ dex for the metallicity. There is also reasonable evidence for the spectroscopic effective temperature scale to be free of systematic errors; typical uncertainties are assessed to ~ 80 K. The basic spectroscopic parameters are supplemented by data for the microturbulence velocities, the projected rotational velocities, stellar radii and α-enhancement abundances, the latter represented by the element magnesium. Stellar masses are also given, though many are probably subject to small adjustments (typically 5%) in forthcoming analyses. The well-defined distance correlation is also demonstrated to be an efficient means for an identification of spectroscopic binaries.

The results are discussed in terms of a spectroscopically established distance scale, the sites of the stellar populations in the [Mg/H]-[Fe/Mg] plane, a timescale for the Galactic thin disk, and the potential of future T_{eff}-$\log g$ *Kiel diagrams* for a precise determination of Galactic globular clusters ages.

Key words: Techniques: spectroscopic – stars: distances – stars: fundamental parameters – stars: late-type – Galaxy: evolution

1. Introduction

One of the most intriguing issues of modern astrophysics refers to the formation and evolution of the Milky Way Galaxy. From stellar evolution we have learned of the general chemical enrichment of matter as a function of time, as witnessed by e.g. the stellar wind of giant stars, the occurrence of planetary nebulae, or the very spectacular supernova events. Nowadays, it is therefore no surprise that the ancient stars of the Galactic halo are found to be metal-poor objects – as opposed to the understanding when they were first analyzed in the 1950s. Interestingly, these stars also reveal a very different kinematic behaviour in that they do not take share in the rotation of the Galactic disk, i.e. they constitute a different *stellar population*, which provides important clues for scenarios of the early epochs.

With the rapidly increased number of observations, the more sophisticated theories, and the very much improved numerical modeling, the last decades saw many distinguished aspects and comprehensive insights into Galactic evolution. Inevitably, and as might have been anticipated, the picture has become progressively complicated, not only in its details, but also in the global characteristics of whether the Galaxy has evolved from *halo-to-bulge* or *halo-to-disk*, whether it evolved from *top-to-bottom*, or, in contradistinction, from *inside-out*, or is actually a combination of both. The role of *accretion* as a major phenomenon has become a substantive issue, convincingly demonstrated by the recent discovery of the Sagittarius dwarf galaxy merger. This striking example, in particular, represents a far-reaching alert to closed box models or other simplified assumptions, in spite of their analytical beauties. Similarly, the system of Galactic globular clusters has been found to be mixed with some foreign intruders, which can alter our notions of, for instance, the instrinsic age spread of the original "founder members" if this polluting subgroup is not accounted for.

The concept of stellar populations has also become more complicated in recent years. Metallicity distributions of the *halo*, the *thick disk* and *thin disk* reveal considerable overlap and do not allow for an unequivocal classification for many stars without reference to other criteria, such as age or kinematics. With respect to the latter, the situation has improved tremendously on the base of the Hipparcos astrometry for nearby stars. But it is also immediately clear that the Hipparcos data take an active part in clarifying the accuracy of stellar age determinations, for they provide detailed measures of the stars' absolute magnitudes. Along with the stellar effective temperature, evolutionary tracks from stellar interior calculations deliver this important datum, and, at the same time, improve our knowledge of the stellar masses. In addition, the combination of effective

---

[*] Based on observations at the German Spanish Astronomical Center, Calar Alto, Spain
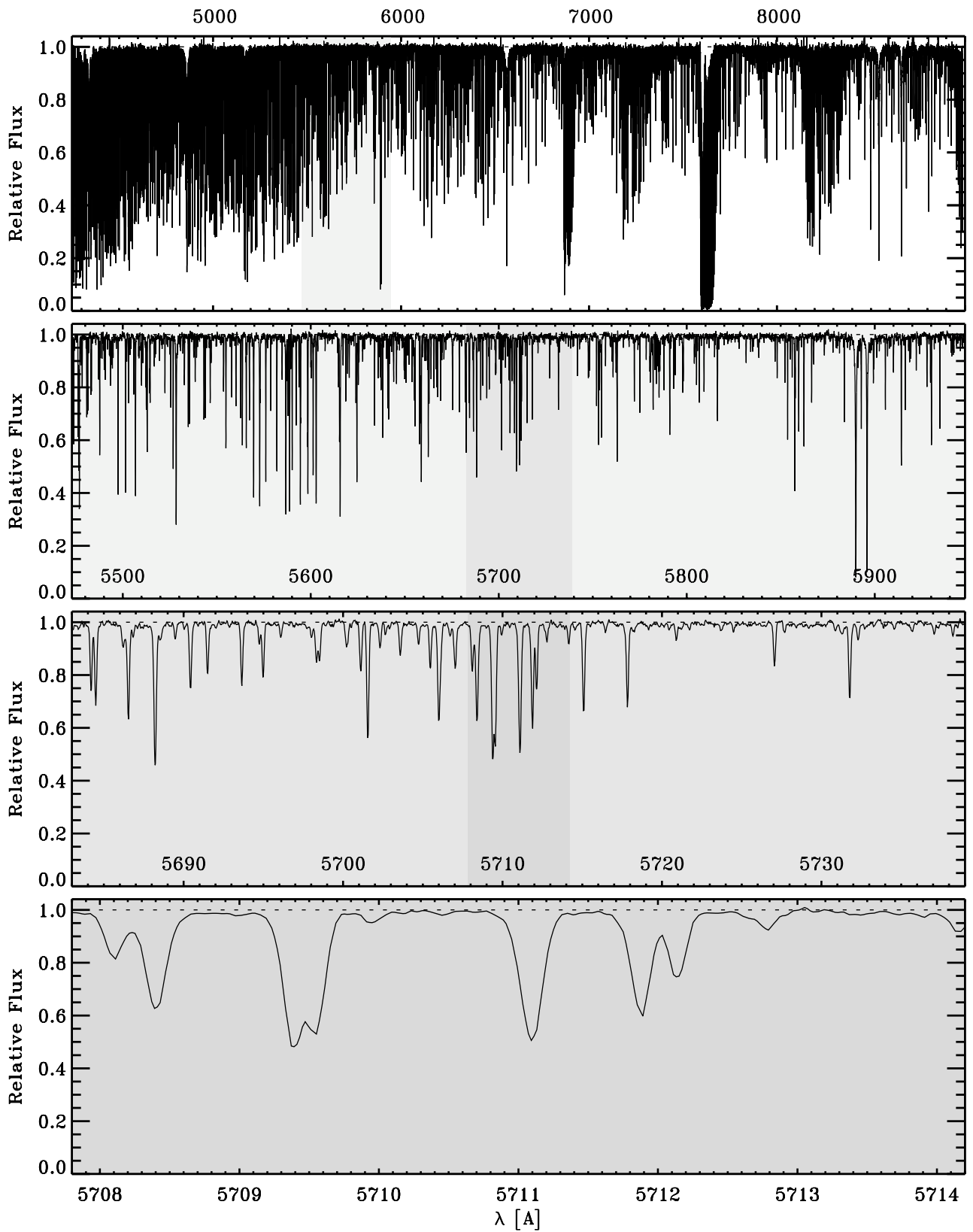
Fig. 1. A FOCES spectrum of the iron-deficient turnoff star ρ CrB with resolution R~60000 and wavelength coverage $\lambda\lambda$4200-9000. The merged échelle spectrum has an equidistant spacing of $\Delta\lambda = 20$mÅ and a total length of $\sim 2 \times 10^5$ data points. The top panel shows the complete spectrum with successive enlargements below

in turn are combined with the masses to provide the surface gravities. Some independent information about this often badly determined parameter is of utmost interest, since it incorporates the important advantage to fix the metallicity scale as well.

For an understanding of the Galactic evolution scenario, rather bright and long-lived stars in not too advanced stages of evolution constitute well-suited candidates. Consequently, we concentrate here on F- and G-type stars of the main-sequence, the turnoff and subgiant region, irrespective of the metal content. Our analysis provides data for approximately fifty nearby stars and is by no means a complete or unbiased sample. Its main purpose is to *explore* the reliability of certain analysis techniques and stellar parameters in different regions of the HR diagram.

In particular, we will confront the spectroscopically deduced parallaxes or distances with the Hipparcos astrometry. From this comparison it will turn out that for certain regions in the HR diagram the surface gravities implied from the LTE iron ionization equilibrium produce conflicting results and we have to recourse to a differential method that employs the wings of strong absorption lines.

Although our sample is not very large, we will present HR diagrams for the *distribution* of the microturbulence parameter ξ_t and the projected rotational velocity, $v\sin i$. In addition, we present data for the stellar radii and masses, although part of the latter may require small corrections on the base of revised evolutionary tracks. Some results are also given for spectroscopic binaries or suspected objects. They were either immediately detected as such from the spectrograms, or, in the course of the analyses, from discrepancies with the distance scale.

Within the last few years several studies were concerned with the metallicity distribution function of the solar neighborhood. For those analyses, where a reasonable number of common objects is present, we confront these data with our findings. A recent sample of stars with effective temperature determinations from the infrared flux method is also compared. Finally, the important behaviour of the magnesium-over-iron abundance as a function of metallicity is discussed and compared to other data from the literature.

2. Observations

The first spectra of our sample were obtained during the implementation phase of the fiber-coupled Cassegrain échelle spectrograph FOCES (Pfeiffer et al. 1998) in September 1995 at the 2.2m and 3.5m telescopes of the Calar Alto Observatory. Those data cover the approximate range 4000-7000Å and were exposed to a 1024^2 24μ CCD at $\lambda/\Delta\lambda \sim 35000$. One year later, in August/September 1996, a similar CCD was employed and observations were done with approximately the same resolution. Then, at the third observing run in October 1996, a new 2048^2 15μ CCD was installed. Although most of this campaign suffered from bad weather conditions, the few available spectra nevertheless convincingly demonstrated the big advantage of the enlarged wavelength coverage (4000-9000Å) and spectral

1997 repeated this setting and supplied about half of the spectra of the present analysis. Fig. 1 gives an illustrative representation for one of the observed stars.

Almost all stars were observed twice, with nominal signal-to-noise values up to ~ 700. Unfortunately, the *real* quality of the data does not exceed S/N~ 200, due to some lasting problems with the fiber interface, that, however, are currently fixed.

3. Stellar atmospheric parameters

We adopt a purely spectroscopic approach. The analysis is strictly differential with respect to the Sun.

The modeling of the spectral lines is based on T. Gehren's (1975) atmosphere program that makes use of the standard assumptions such as hydrostatic equilibrium, plane-parallel layers and local thermodynamic equilibrium, and is fed by the opacity distribution functions described in Kurucz (1992) for an inclusion of the effects of line blanketing. The underlying abundance pattern assumes either a solar mixture close to the one given in Grevesse, Noels & Sauval (1996) or the so-called α-enhancement. The latter is a well-known feature of many metal-poor stars that tend to be overabundant by approximately 0.4 dex in α-chain nuclei O, Ne, Mg, Si, S, Ar, Ca and probably Ti. Hence, basically two grids of model atmospheres encompass our program stars for values in T_{eff} and log g as displayed in the *Kiel diagram* of Fig. 2 and for about five orders of magnitude in metallicity, up to [Fe/H]$= +1.0$.

Effective temperatures are deduced from the wings of the Balmer lines, since they are very sensitive to this parameter in our temperature range (e.g. Schmidt 1972). Surface gravities are usually derived from the ionization equilibria of abundant species, we focus here on the most often used iron. In addition, the wings of strong lines, such as the Mg Ib triplet, are also well-known to represent pressure-dependent features and may serve as a diagnostics for the surface gravity parameter (e.g. Deeming 1960). It is important to realize that values of T_{eff} and log g are interdependent if the latter is derived from the ionization equilibrium, whereas both stellar parameters are rather decoupled if we make use of the Mg Ib lines. This may have advantages and disadvantages, as we will see in what follows.

Once the gravity parameter is fixed from the ionization equilibrium method, a value for the iron abundance is provided as well. But this result depends on lines of neutral iron, which are known to be sensitive to NLTE effects, details of the model atmosphere structures, as well as the value deduced for the effective temperature. A discrepant result for the log g parameter, from e.g. a comparison with the Hipparcos astrometry, provides an almost certain evidence for an erroneous abundance scale. Singly ionized iron lines, on the contrary, may exclusively be employed in combination with the strong line method. They are assumed to be formed under LTE conditions and are less affected by details of the temperature structure, since they reside in the principal stage of ionization for F and G dwarfs. A drawback of this species nevertheless results from the fact that only a handful of suitable absorption features is available
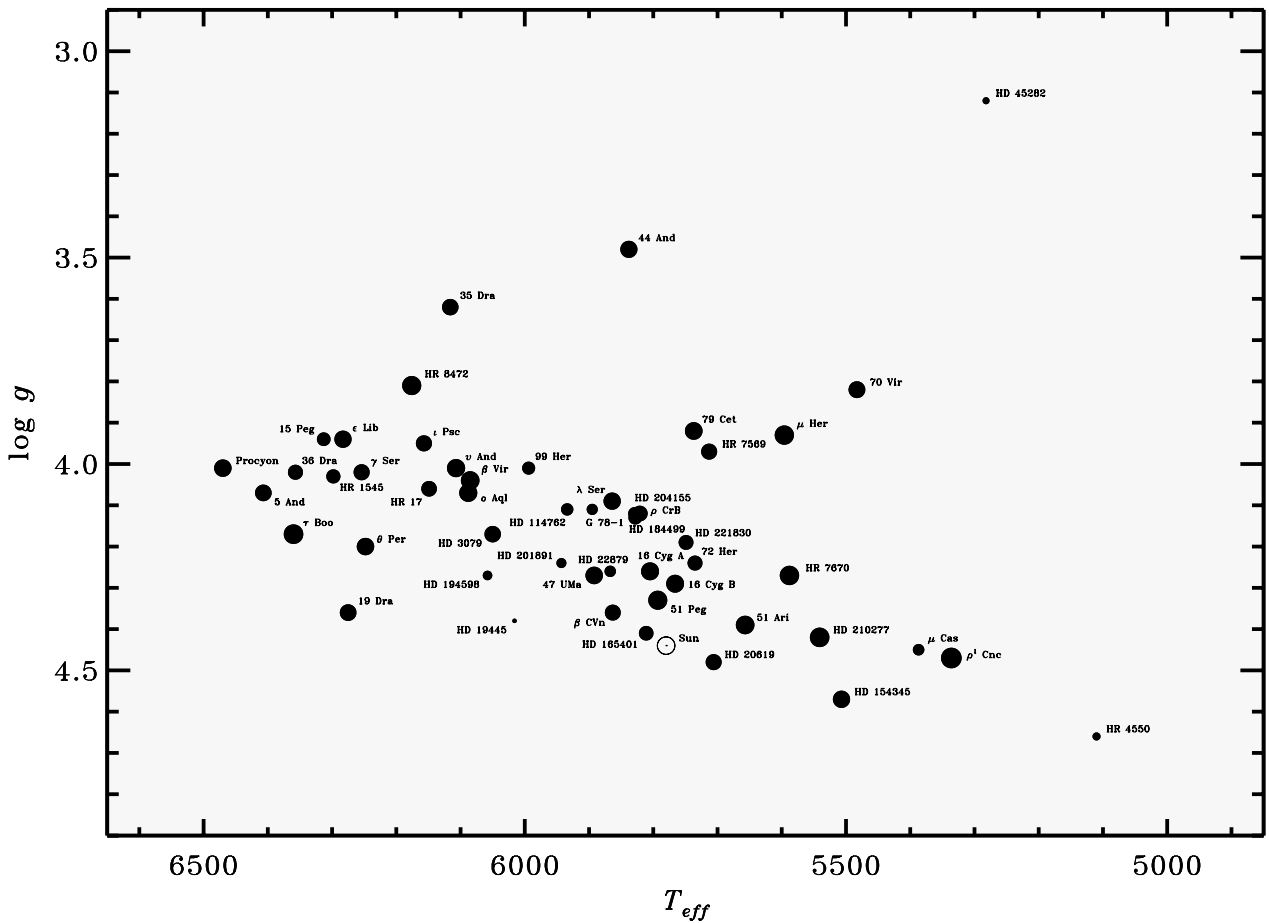
Fig. 2. The T_{eff}-log g *Kiel diagram* of the program stars. Circle diameters are in proportion to the metallicities

in the visible and Fe II lines reveal the somewhat disadvantageous dependence on the exact elemental mixture, that is, the *relative* overabundance of α-elements, notably magnesium and silicon, has to be taken into account. Both of these elements can release substantial amounts of electrons to the photosphere, which in turn affect the continuous H^- opacity, and hence the line formation.

Another circumstance that hampers a correct abundance determination from stellar spectra has to do with the presence of a non-thermal velocity component that acts as an extra absorber to the metal lines. If not taken into account, the inferred metal abundances depend on the measured equivalent widths of individual lines. This undesirable behaviour is usually overcome by the introduction of an additional atmospheric parameter, the *microturbulence*, aptly chosen if all absorption lines of a certain species produce the same abundance. In a differential investigation, we derive this velocity parameter from profile analyses of selected Fe I and Fe II lines of the solar spectrum, along with the individual oscillator strengths and damping constants. The underlying laboratory is realized by the tracings of the Kitt Peak Solar Flux Atlas (Kurucz et al. 1984) from which we infer a microturbulence velocity $\xi_t = 0.90 \pm 0.15$ km s^{-1}. In view

of the many details displayed in the extremely resolved solar atlas, this value for the microturbulence inevitably comes out as a compromise to our incomplete modeling abilities and, of course, refers to the employed atlas and model atmosphere. Other combinations, such as the often used solar intensity spectra, will certainly show up different results. But as long as the analysis is done in a consistent and differential manner, there is the justified hope that the microturbulence values obtained for other stars give rise to a reliable abundance scale that keeps systematic errors to a minimum.

If we employ the Kitt Peak Solar Flux Atlas as the primary reference, another important advantage results from the fact that Moon spectra, acquired with the same settings as the program stars, can be compared with the convolved solar spectrum to derive the respective *instrumental profiles*.

There are at least two other large scale motions that contribute to the observed line profiles: (i) *stellar rotation*, or, more precise, the *projected rotational velocity* $v\sin i$, with i as the usually unknown inclination angle, and (ii) the so-called *macroturbulence*, the phenomenon that causes the wiggly lines in spatially resolved spectra of the Sun. Unfortunately, both effects involve velocity fields that are of comparable strength

that well resolved (in particular those obtained before October 1996) as to put real constraints on either quantity. On the other hand, studies of macroturbulence velocities have revealed a smooth behaviour along the T_{eff}-$\log g$ plane of our program stars. Whether metallicity or age do have a major impact is not that clear, but metal-poor stars are normally very slow rotators, which is a very useful information, when considering the individual contributions of macroturbulence and rotation for certain stars. In our work we employ the macroturbulence parameter ζ in the radial-tangential form and adopt values as prescribed in Gray (1984, 1992), with some allowance to slightly smaller values (~ 0.5 km s^{-1}) for stronger lines (cf. Gray 1977). Along with the known instrumental profile, the projected rotational velocities are then obtained as the residuals to the observed line profiles. It turns out, that eventually a few metal-poor stars with negligible $v\sin i$'s require somewhat lower ζ_{RT} values than proposed by Gray's work.

As a final remark, we note that the atmospheric parameters presented in this work are by no means obtained in a straightforward manner. Several steps are subject to iterative procedures and almost every star is observed and analyzed twice. Others, like the bright F5 star *Procyon* and the Moon, were repeatedly monitored for an intercomparison of different observing runs as well as different spectrograph settings. The results are encouraging in that redundant observations provide stellar atmospheric parameters with fairly small intrinsic scatter. This situation was again improved with the introduction of the 15μ CCD in October 1996, and further developments are expected for the next observing seasons, as soon as the fiber interface will achieve the expected performance.

4. Results

Before we consider individual results in more detail, we give a description of Table 1 that summarizes the relevant data. Each star is represented in two consecutive rows, one for the stellar parameters and the other for the corresponding error estimates. Columns (1) – (3) give the object names and/or catalogue numbers. The apparent visual magnitudes in column (4) are taken from Mermilliod, Mermilliod & Hauck (1997). The next three columns tabulate the basic atmospheric parameters T_{eff}, $\log$ g and [Fe/H], supplemented by the microturbulence ξ_t in column (8) and the [Mg I/Fe I] abundance denoted as "Mg" in column (9). Error estimates for the surface gravities, the microturbulence values and the magnesium-over-iron abundances are generally assumed to be 0.1 dex, 0.2 dex, and 0.05 dex, respectively; the effective temperatures and metallicities have typical errors of $\Delta T_{eff} \sim 80$ K and Δ[Fe/H]~ 0.07 dex. As explained in the preceding section, the macroturbulence values ζ_{RT} in column (10) are generally taken from Gray (1984, 1992) with only minor corrections for few metal-poor stars. The $v\sin i$ values in column (11) are derived from the line profile analyses, but they have to be considered in conjunction with the ζ_{RT} values of the preceding column. The absolute bolometric magnitudes in column (12) are calculated from the

bolometric corrections of column (13); the latter are taken from Alonso, Arribas & Martínez-Roger (1995) for which we adopt $\Delta BC_V \simeq 0.05$ mag as a representative error for all stars. Interstellar extinction is usually found to be negligible, except for HD 45282, the most distant star of the sample, where $A_V \sim 0.10$ is indicated from Strömgren photometry. As mentioned in the Introduction, many of the stellar masses in column (14) are presumably subject to small corrections, typically 5%. The tabulated data are either taken from $\log T_{eff}$-M_{bol} isochrones of Bergbusch & VandenBerg (1992), or recent calculations of J. Bernkopf (private communication). The general uncertainties of the stellar masses are assessed to be less than 10%. The stellar radii in column (15) are immediately obtained from the effective temperatures and bolometric magnitudes. Finally, the last three columns (16) – (18) compare the spectroscopic distance scale with the Hipparcos astrometry on the base of the data of the preceding columns.

At the end of Table 1 two groups of stars are listed separately. First, suspected spectroscopic binaries or variable stars, suggested as such from inconsistencies with the Hipparcos parallaxes, and, second, a few objects that could not be analyzed for the (suspected) presence of a companion spectrum.

We complete the description of Table 1 with a few general remarks on the given error estimates. To be specific, we ask whether *internal* or *external* errors should be tabulated. Neither choice is probably a good one, because internal errors tend to be very small with little relevance to the physical quantity, whereas errors claimed to be "external" have often turned out to be a fake. The recent Hipparcos data have shown some striking examples in this respect.
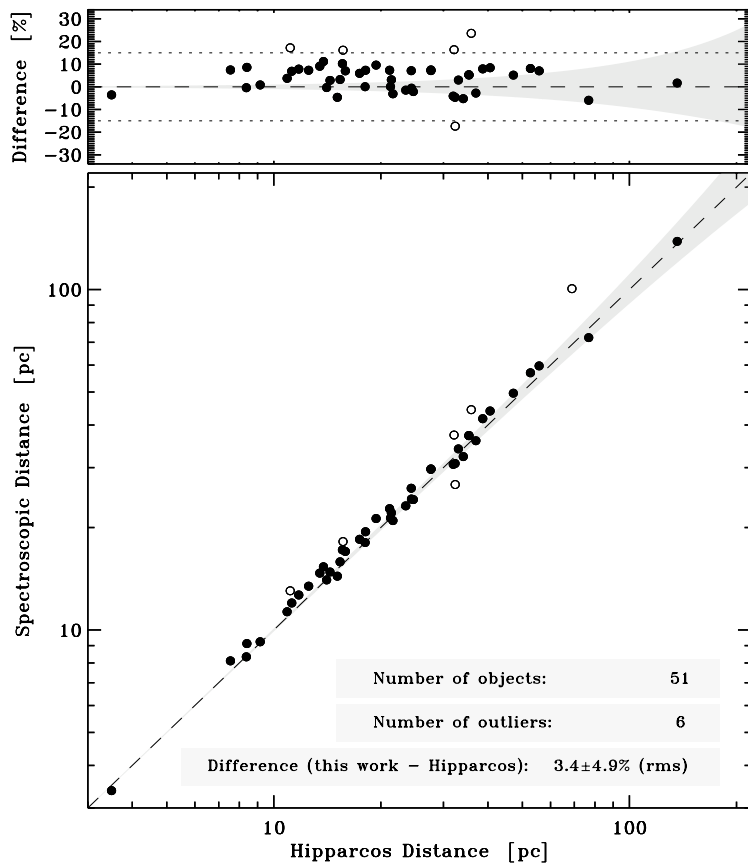
To exemplify this difficulty we consider the data for the metallicity in column (7): many of our spectra are investigated for about 30 Fe I and 10 Fe II lines. They provide an internal error of the mean of usually less than 0.01 dex and even the *rms* error is typically smaller than 0.03 dex. If, however, we repeat the analyses with a second spectrum of the same star the results often differ by the same 0.03 dex, that is, the error of the mean certainly has little or no meaning. But also the 0.03 dex *rms* error corresponds to less than ~ 1.5 mÅ for many of the investigated iron lines. This is in fact a very small amount and though it is pleasing to be statistically that precise with the modern solid state detectors, does this value necessarily imply a meaningful measure for the accuracy of the star's metallicity? We hesitate to flag this parameter with such a small uncertainty. Instead, it seems more reasonable to give an error estimate that is not too formal or too optimistic, and not the worst case scenario. The main driving force should rather be the inexperienced "user" of the data, who is asking to what extent one might apply or trust the results with our current understanding.

In this respect the error estimates of Table 1 are neither internal nor external, but the subjective assessment of the general quality that emerged in the course of this work. If known systematic effects are likely to come into play we have tried to mention these restrictions in the relevant discussions of the individual parameters.

Table 1. Stellar parameters of the program stars. Most of the entries are self-explanatory; Mg denotes the [Mg I/Fe I] abundance, d_{HIP} in column (16) is the Hipparcos distance, d_{sp} in column (17) the spectroscopically deduced value, Δd the difference of both. For each star the second row indicates the error estimates. The macroturbulence value ζ_{RT} is generally *adopted* according to the relations given in Gray (1984, 1992), with only few small adjustments for metal-poor stars. The bolometric magnitudes in column (12) are based on the Hipparcos parallaxes, with bolometric corrections taken from Alonso, Arribas & Martínez-Roger (1995) and tabulated in column (13). Errors of $\log g$, ξ_t, [Mg I/Fe I] and BC_V are estimated to be 0.1 dex, 0.2 dex, 0.05 dex and 0.05 dex, respectively. Uncertainties for the stellar masses are expected to be less than 10%. At the end of the table two groups of stars are listed separately: first, the six objects – depicted by open circles in Fig. 3 – that are considered as outliers, and, second, stars that could not be analyzed for their putative or definite presence of a companion spectrum

(1)	(2)	(3)	(4)	(5)	(6)	(7)	(8)	(9)	(10)	(11)	(12)	(13)	(14)	(15)	(16)	(17)	(18)
Object	HR	HD	V	T_{eff} [K]	$\log g$	[Fe/H]	ξ_t [km/s]	Mg	ζ_{RT} [km/s]	$v\sin i$ [km/s]	M_{bol}	BC_V	Mass $[M_\odot]$	Radius $[R_\odot]$	d_{HIP} [pc]	d_{sp} [pc]	Δd [%]
	17	400	6.190	6149	4.06	−0.25	1.31	+0.08	5.6	4.3	3.49	−0.10	1.09	1.57	33.05	34.03	3.0
			0.061	80	0.10	0.07	0.20	0.05		0.8	0.09	0.05		0.08	0.77	4.76	
		3079	7.376	6050	4.17	−0.14	1.42	+0.06	5.1	2.3	3.90	−0.11	1.07	1.34	47.17	49.60	5.1
			0.009	80	0.10	0.07	0.20	0.05		1.0	0.10	0.05		0.08	2.02	6.80	
μ Cas	321	6582	5.163	5387	4.45	−0.83	0.89	+0.42	2.0	1.0	5.54	−0.23	0.75	0.80	7.55	8.12	7.4
			0.016	80	0.10	0.08	0.20	0.05		1.0	0.05	0.05		0.03	0.03	1.12	
44 And	340	6920	5.661	5838	3.48	−0.05	1.35	+0.06	4.9	11.6	1.93	−0.12	1.64	3.58	52.69	56.94	8.1
			0.010	80	0.10	0.09	0.20	0.05		0.8	0.10	0.05		0.19	2.05	7.82	
υ And	458	9826	4.086	6107	4.01	+0.09	1.40	+0.03	5.4	9.5	3.36	−0.08	1.27	1.69	13.47	14.69	9.1
			0.013	80	0.10	0.06	0.20	0.05		0.8	0.06	0.05		0.06	0.13	2.01	
θ Per	799	16895	4.107	6248	4.20	−0.01	1.42	+0.01	5.8	9.1	3.78	−0.08	1.17	1.33	11.23	12.00	6.9
			0.017	80	0.10	0.07	0.20	0.05		0.8	0.06	0.05		0.05	0.10	1.65	
51 Ari		18803	6.616	5657	4.39	+0.14	0.87	−0.01	3.1	2.0	4.84	−0.15	1.02	1.00	21.16	22.71	7.3
			0.022	80	0.10	0.07	0.20	0.05		1.0	0.07	0.05		0.04	0.41	3.13	
		19445	8.054	6016	4.38	−1.95	1.35	+0.46	4.2	1.0	4.91	−0.21	0.74	0.85	38.68	41.75	7.9
			0.023	80	0.10	0.07	0.20	0.05		1.0	0.11	0.05		0.05	1.78	5.74	
		20619	7.044	5706	4.48	−0.20	0.90	+0.02	3.3	1.5	4.93	−0.15	0.93	0.94	24.68	24.16	−2.1
			0.021	70	0.10	0.07	0.20	0.05		1.0	0.08	0.05		0.04	0.61	3.31	
		22879	6.689	5867	4.26	−0.84	1.21	+0.43	4.2	1.0	4.59	−0.17	0.82	1.04	24.35	26.08	7.1
			0.009	80	0.10	0.07	0.20	0.05		1.0	0.07	0.05		0.04	0.52	3.58	
	1545	30743	6.260	6298	4.03	−0.45	1.64	+0.14	6.1	5.1	3.41	−0.10	1.04	1.55	35.36	37.25	5.3
			0.009	80	0.10	0.07	0.20	0.05		1.0	0.08	0.05		0.07	1.03	5.10	
		45282	8.029	5282	3.12	−1.52	1.43	+0.37	4.2	1.0	1.98	−0.28	0.90	4.26	136.24	138.55	1.7
			0.008	80	0.10	0.06	0.20	0.05		1.0	0.31	0.05		0.66	20.50	19.10	
Procyon	2943	61421	0.367	6470	4.01	−0.01	1.91	+0.06	6.8	2.6	2.59	−0.06	1.60	2.15	3.50	3.37	−3.6
			0.010	80	0.10	0.07	0.20	0.05		1.0	0.05	0.05		0.07	0.01	0.46	
ρ^1 Cnc	3522	75732	5.942	5336	4.47	+0.40	0.76	+0.00	1.9	2.5	5.23	−0.22	1.08	0.94	12.53	13.45	7.3
			0.015	90	0.10	0.07	0.20	0.05		1.0	0.06	0.05		0.04	0.13	1.87	
47 UMa	4277	95128	5.051	5892	4.27	+0.00	1.01	+0.00	4.0	1.5	4.19	−0.12	1.03	1.24	14.08	14.03	−0.3
			0.016	70	0.10	0.07	0.20	0.05		1.0	0.06	0.05		0.04	0.13	1.92	
β Vir	4540	102870	3.608	6085	4.04	+0.14	1.38	+0.01	5.2	2.5	3.34	−0.08	1.27	1.72	10.90	11.31	3.8
			0.010	80	0.10	0.09	0.20	0.05		1.0	0.05	0.05		0.06	0.09	1.55	
	4550	103095	6.446	5110	4.66	−1.35	0.85	+0.28	1.0	1.5	6.33	−0.31	0.64	0.62	9.16	9.23	0.8
			0.009	80	0.10	0.10	0.20	0.05		1.0	0.05	0.05		0.02	0.07	1.28	
β CVn	4785	109358	4.260	5863	4.36	−0.21	1.12	+0.07	4.1	1.8	4.51	−0.13	0.96	1.08	8.37	8.34	−0.4
			0.007	70	0.10	0.06	0.20	0.05		1.0	0.05	0.05		0.04	0.06	1.14	
		114762	7.308	5934	4.11	−0.71	1.14	+0.33	4.1	1.0	4.12	−0.15	0.88	1.27	40.57	43.98	8.4
			0.013	80	0.10	0.08	0.20	0.05		1.0	0.14	0.05		0.09	2.52	6.04	
70 Vir	5072	117176	4.975	5483	3.82	−0.09	1.02	+0.08	3.9	1.5	3.50	−0.19	1.07	1.97	18.11	19.43	7.3
			0.008	80	0.10	0.07	0.20	0.05		1.0	0.06	0.05		0.08	0.24	2.67	
τ Boo	5185	120136	4.496	6360	4.17	+0.27	1.56	+0.00	6.3	15.6	3.48	−0.05	1.42	1.48	15.60	17.19	10.2
			0.008	80	0.10	0.08	0.20	0.05		0.7	0.06	0.05		0.05	0.17	2.35	
λ Ser	5868	141004	4.426	5864	4.09	−0.03	1.05	+0.02	4.4	2.0	3.95	−0.12	1.01	1.39	11.75	12.67	7.8
			0.009	70	0.10	0.06	0.20	0.05		1.0	0.05	0.05		0.05	0.11	1.73	
ρ CrB	5968	143761	5.412	5821	4.12	−0.24	1.10	+0.19	4.1	1.0	4.07	−0.14	0.97	1.34	17.43	18.47	6.0
			0.016	80	0.10	0.08	0.20	0.05		1.0	0.06	0.05		0.05	0.22	2.54	
19 Dra	6315	153597	4.889	6275	4.36	−0.11	1.48	+0.01	5.6	8.9	3.91	−0.09	1.17	1.24	15.09	14.39	−4.6
			0.016	80	0.10	0.08	0.20	0.05		0.8	0.05	0.05		0.05	0.11	1.97	
		154345	6.765	5507	4.57	−0.03	0.70	−0.03	2.5	2.4	5.30	−0.18	0.98	0.85	18.06	18.07	0.1
			0.012	80	0.10	0.07	0.20	0.05		1.0	0.06	0.05		0.03	0.18	2.49	

(1) Object	(2) HR	(3) HD	(4) V	(5) T_{eff} [K]	(6) $\log g$	(7) [Fe/H]	(8) ξ_t [km/s]	(9) Mg	(10) ζ_{RT} [km/s]	(11) $v\sin i$ [km/s]	(12) M_{bol}	(13) BC_V	(14) Mass [$M_\odot$]	(15) Radius [$R_\odot$]	(16) d_{HIP} [pc]	(17) d_{sp} [pc]	(18) Δd [%]
72 Her	6458	157214	5.394	5735	4.24	–0.34	1.00	+0.38	3.7	1.0	4.45	–0.15	0.90	1.16	14.39	14.80	2.8
			0.013	80	0.10	0.07	0.20	0.05		1.0	0.05	0.05		0.04	0.12	2.03	
μ Her	6623	161797	3.417	5596	3.93	+0.23	1.17	+0.00	4.1	1.0	3.64	–0.15	1.14	1.77	8.40	9.12	8.6
			0.014	80	0.10	0.07	0.20	0.05		1.0	0.05	0.05		0.07	0.04	1.26	
		165401	6.804	5811	4.41	–0.39	1.10	+0.33	3.8	2.0	4.72	–0.15	0.92	1.00	24.39	24.25	–0.6
			0.008	80	0.10	0.08	0.20	0.05		1.0	0.07	0.05		0.04	0.53	3.33	
36 Dra	6850	168151	5.022	6357	4.02	–0.33	1.68	+0.13	6.3	9.2	3.07	–0.09	1.17	1.78	23.50	23.16	–1.4
			0.018	80	0.10	0.07	0.20	0.05		0.8	0.06	0.05		0.07	0.25	3.17	
		184499	6.628	5828	4.13	–0.51	1.17	+0.40	4.2	1.0	3.95	–0.15	0.90	1.41	31.96	30.66	–4.1
			0.011	80	0.10	0.07	0.20	0.05		1.0	0.07	0.05		0.06	0.65	4.21	
16 Cyg A	7503	186408	5.960	5805	4.26	+0.06	1.03	+0.01	3.9	2.0	4.16	–0.12	1.04	1.29	21.62	20.96	–3.1
			0.009	60	0.10	0.05	0.20	0.05		1.0	0.06	0.05		0.04	0.24	2.85	
16 Cyg B	7504	186427	6.215	5766	4.29	+0.05	0.89	+0.03	3.7	1.5	4.43	–0.13	1.01	1.16	21.41	22.08	3.1
			0.014	60	0.10	0.05	0.20	0.05		1.0	0.06	0.05		0.04	0.24	3.01	
o Aql	7560	187691	5.116	6088	4.07	+0.07	1.35	+0.03	5.2	3.0	3.59	–0.09	1.20	1.53	19.39	21.25	9.6
			0.005	80	0.10	0.08	0.20	0.05		0.9	0.06	0.05		0.06	0.29	2.91	
	7569	187923	6.142	5713	3.97	–0.20	1.19	+0.19	4.0	1.5	3.78	–0.15	0.99	1.59	27.66	29.72	7.4
			0.015	80	0.10	0.10	0.20	0.05		1.0	0.07	0.05		0.07	0.62	4.09	
	7670	190360	5.730	5588	4.27	+0.24	0.98	+0.03	3.1	2.8	4.57	–0.16	1.04	1.16	15.89	17.01	7.0
			0.023	80	0.10	0.08	0.20	0.05		1.0	0.06	0.05		0.05	0.16	2.35	
		194598	8.345	6058	4.27	–1.12	1.45	+0.29	4.6	1.0	4.45	–0.17	0.84	1.04	55.74	59.66	7.0
			0.010	80	0.10	0.07	0.20	0.05		1.0	0.16	0.05		0.09	4.14	8.18	
		201891	7.373	5943	4.24	–1.05	1.18	+0.41	4.5	1.0	4.46	–0.17	0.81	1.08	35.39	37.22	5.2
			0.011	80	0.10	0.08	0.20	0.05		1.0	0.09	0.05		0.06	1.31	5.11	
		204155	8.495	5829	4.12	–0.63	1.18	+0.41	4.2	1.0	3.91	–0.16	0.88	1.44	76.80	72.26	–5.9
			0.009	80	0.10	0.08	0.20	0.05		1.0	0.20	0.05		0.14	7.16	9.92	
15 Peg	8354	207978	5.532	6313	3.94	–0.52	1.57	+0.21	6.2	6.8	3.21	–0.11	1.04	1.69	27.66	29.64	7.1
			0.015	80	0.10	0.07	0.20	0.05		0.8	0.07	0.05		0.07	0.54	4.06	
		210277	6.590	5541	4.42	+0.26	0.73	–0.01	2.6	2.0	4.78	–0.17	1.09	1.07	21.29	21.31	0.1
			–	80	0.10	0.07	0.20	0.05		1.0	0.06	0.05		0.04	0.36	2.93	
	8472	210855	5.251	6176	3.81	+0.21	1.61	+0.02	5.7	11.5	2.34	–0.07	1.55	2.64	37.00	35.98	–2.7
			0.015	80	0.10	0.06	0.20	0.05		0.8	0.07	0.05		0.11	0.68	4.93	
51 Peg	8729	217014	5.463	5793	4.33	+0.20	0.95	–0.03	3.7	2.0	4.41	–0.12	1.11	1.16	15.36	15.85	3.2
			0.020	70	0.10	0.07	0.20	0.05		1.0	0.06	0.05		0.04	0.18	2.17	
5 And	8805	218470	5.680	6407	4.07	–0.12	1.85	+0.07	6.4	13.1	2.94	–0.07	1.33	1.86	34.09	32.32	–5.2
			0.029	80	0.10	0.08	0.20	0.05		1.0	0.07	0.05		0.08	0.74	4.44	
		221830	6.851	5749	4.19	–0.36	1.14	+0.38	3.6	1.0	4.15	–0.15	0.90	1.33	32.33	30.84	–4.6
			0.008	80	0.10	0.07	0.20	0.05		1.0	0.07	0.05		0.06	0.78	4.24	
ι Psc	8969	222368	4.124	6157	3.95	–0.19	1.51	+0.09	5.6	5.1	3.33	–0.10	1.14	1.69	13.79	15.33	11.2
			0.006	80	0.10	0.07	0.20	0.05		1.0	0.06	0.05		0.06	0.17	2.10	
79 Cet		16141	6.832	5737	3.92	+0.02	1.24	+0.04	4.2	1.0	3.92	–0.13	1.01	1.48	35.91	44.38	23.6
			0.014	70	0.10	0.08	0.20	0.05		1.0	0.12	0.05		0.09	1.89	6.07	
G 78–1			9.160	5895	4.11	–0.88	1.14	+0.38	4.5	1.0	4.80	–0.17	0.87	0.93	68.92	100.62	46.0
			0.000	90	0.10	0.08	0.20	0.05		1.0	0.21	0.05		0.10	6.67	13.87	
ϵ Lib	5723	137052	4.929	6283	3.94	–0.03	1.89	+0.08	6.5	10.2	2.30	–0.08	1.46	2.60	32.36	26.75	–17.4
			0.005	80	0.10	0.08	0.20	0.05		0.8	0.09	0.05		0.13	1.07	3.66	
γ Ser	5933	142860	3.842	6254	4.02	–0.19	1.36	+0.04	5.9	10.6	3.52	–0.09	1.17	1.50	11.12	13.03	17.2
			0.018	80	0.10	0.07	0.20	0.05		0.8	0.06	0.05		0.06	0.09	1.79	
35 Dra	6701	163989	5.033	6116	3.62	–0.14	1.61	+0.05	5.7	2.0	2.40	–0.10	1.41	2.62	32.12	37.38	16.4
			0.027	80	0.10	0.07	0.20	0.05		1.0	0.07	0.05		0.11	0.49	5.14	
99 Her	6775	165908	5.047	5994	4.01	–0.61	1.25	+0.18	4.6	1.0	3.93	–0.14	0.91	1.35	15.65	18.18	16.2
			0.013	80	0.10	0.07	0.20	0.05		1.0	0.05	0.05		0.05	0.14	2.49	
	5534	130948	5.855	–	–	–	–	–	–	–	–	–	–	–	17.94	–	–
			0.005	–	–	–	–	–	–	–	–	–	–	–	0.26	–	
	7955	198084	4.513	–	–	–	–	–	–	–	–	–	–	–	27.12	–	–
			0.012	–	–	–	–	–	–	–	–	–	–	–	0.34	–	
		201889	8.055	–	–	–	–	–	–	–	–	–	–	–	55.71	–	–
			0.015	–	–	–	–	–	–	–	–	–	–	–	4.86	–	

Suspected binaries or variable stars:

G 78−1	at	68 pc	with	8.69 σ
ϵ Lib	at	32 pc	with	4.24 σ
79 Cet	at	35 pc	with	4.11 σ
γ Ser	at	11 pc	with	2.81 σ
35 Dra	at	32 pc	with	2.64 σ
99 Her	at	15 pc	with	2.60 σ

Fig. 3. Comparison of the spectroscopic versus astrometric distance scale. Errors in the Hipparcos data are negligible below 10 pc, comparable around 100 pc and get worse beyond; the shaded wedge illustrates this behaviour for a typical parallax error of 1 mas. Statistical corrections to account for the possible bias in the astrometric data of the few more distant objects are very small and therefore neglected. Individual uncertainties of the spectroscopic data are about 10-15% (dotted curve), with no dependence on distance. The spectroscopic distances result in *higher* values by 3.4% on average, and a statistical *rms* error of 4.9%. The corresponding offset in the surface gravity parameter – to which this result is most susceptible – is $\Delta \log g \sim 0.03$ dex. Consequently, the accuracy of the well-defined correlation reveals several outliers (open circles), most of which are supposed to be spectroscopic binaries. By means of an iterative 3σ criterion three deviating stars are immediately identified: 79 Cet at 4.11σ, ϵ Lib at 4.24σ, and G 78–1 at 8.69σ; the latter two are in fact known as spectroscopic binaries. Three other stars, γ Ser, 35 Dra and 99 Her, are slightly below the 3σ threshold. The weakest case, 99 Her at 2.60σ, is however a well-known visual binary (P$\sim$56 yr) that was separated by only a few tenths of an arcsec at the time of observation (see text for details)

4.1. Discussion of the stellar parameters

We commence with the discussion of Fig. 3 that compares our spectroscopically deduced distances with the solid space-borne astrometry of the Hipparcos satellite. The analyses of the stellar spectra leads to the determination of the effective temperatures, surface gravities and metallicities. Application to evolutionary tracks yields the stellar masses, and along with the apparent bolometric magnitudes of the stars, the calculation of *spectroscopic parallaxes* is feasible and provides a very decisive test to our notions of the precision of modeling, especially if the underlying astrometric scale is that well established.

In this respect we consider Fig. 3 to be a very encouraging result for the quality of our current model atmosphere analyses that is reassuring for further work to come in the era of the forth-coming large telescopes. The well-defined distance correlation basically confirms *the accuracy of the surface gravity determinations*, to which Fig. 3 is most susceptible: the systematic deviation of 3.4% translates to a $\Delta \log g$ of only 0.03 dex! As opposed to this, surface gravities of F stars at the turnoff can easily show discrepant results of $\sim$0.4 dex if derived from the usually employed LTE iron ionization equilibrium.

In Fig. 4 we display this finding in the T_{eff}-$\log g$ plane, where surface gravity parameters derived from the LTE iron ionization equilibrium method are compared to the strong line method (here, and in what follows, the six deviating open circle stars of Fig. 3 are omitted). As is immediately obvious, the discrepancies increase towards hotter stars, i.e. they must be affiliated with either NLTE effects of Fe I lines or an incomplete
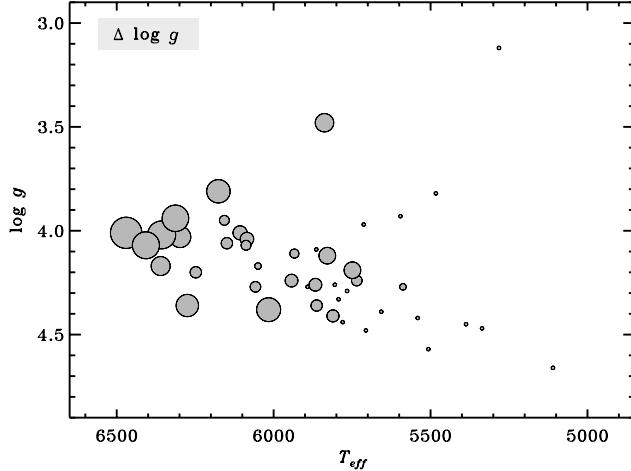
Fig. 4. Deviations in the *spectroscopic* log g determinations between the ionization equilibrium method and the strong line method in the *Kiel diagram*. Circle diameters are in proportion to the derived discrepancies (for an identification of individual objects the reader should consult Fig. 2). Cool stars, on either the main-sequence or in evolved stages of evolution, reveal no significant deviations. Hotter stars, and in particular many turnoff objects, are however notably affected. The largest circle in the diagram corresponds to $\Delta \log g \sim 0.45$ dex. There is also some indication that metal-poor stars require larger $\Delta \log g$ corrections (cf. HD 19445)

modeling of the underlying atmospheres to which these lines are very sensitive in this temperature range.

On the other hand, the diagram shows consistent results with both log g methods for the late-type stars. Even more it turns out that our data for the strong line method reveal a convergence behaviour for the log g corrections that deteriorates towards the coolest of the investigated stars. This is however not a principal drawback of the method. It merely results from the fact that the two important Mg I lines $\lambda 4571$ and $\lambda 5711$, which are normally weak and thereby serve to fix the Mg I abundance, increase in strength and develop pressure-dependent line wings on their own. In addition, the problem of line blends becomes severe for late-G and K stars, and requires a complete profile synthesis of all relevant lines for the study of the Mg Ib line wings. The cool main-sequence star HR 4550, also known as Gmb 1830, to the very right in Fig. 4, was actually not analyzed by means of the strong Mg Ib lines for exactly this reason, although this is a metal-poor halo star with [Fe/H]$= -1.35$.

In practice we employed both log g methods for stars of approximately solar effective temperature, discarded the results of the iron ionization equilibrium for the hotter stars, but made use of it with increasing weight towards the late-type stars.

The applicability of the iron ionization equilibrium method for the cool stars of the sample has an important impact on the assessment of the reliability of the Balmer lines as an effective temperature indicator for these objects. If, for instance, we would adopt an effective temperature for HR 4550 that deviates by 100 K from our preferred value, this causes a shift in log g

scale. This is however not observed in Fig. 3 for any of the cool stars, regardless of the metal content or evolutionary stage. As a result, the Hipparcos data provide convincing evidence that the Balmer-line-based effective temperatures are most likely *unaffected by systematic errors in this temperature range*. Unfortunately, the decoupling of the methods for the T_{eff} and log g determinations of the hotter stars makes no allowance for a similar precise statement on the effective temperature scale of the investigated F stars. Note however, that our effective temperature value for the F5 star *Procyon* at the very hot end of the sample is not in conflict with existing results from direct diameter measurements (e.g. Code et al. 1976). Nevertheless some interferometric data for at least one metal-poor star at the turnoff would be very welcome.

With the information of a fairly well determined surface gravity scale, we can now attempt to address the accuracy of the stellar *metallicities*. Since we take only Fe II lines into account for the hotter stars, and Fe I lines in only those cases when the Fe I/II ionization equilibrium results in non-discrepant surface gravity values, NLTE effects or existing shortcomings of the model atmospheres are unlikely to have a significant impact. Uncertainties in the effective temperature scale for the hotter stars also pose no difficulties, since the employed Fe II lines are almost unaffected by changes of e.g. 100 K. Uncertainties in the effective temperature scale for the cooler stars can be excluded for the close coupling with the surface gravities as explained above. If the 3.4% systematic deviation of the distance scale in Fig. 3 is exclusively related to the surface gravity parameter, the corresponding $\Delta \log g \sim 0.03$ dex discrepancy propagates into a mere Δ[Fe/H]~ 0.02 dex in metallicity. One possible source of error may however affect the analyses of the faster rotating ($v\sin i > 10$ km s^{-1}) F stars that could lead to artificial overabundances as a result of line blending. Similarly, careful line profile analyses are required for metal-rich stars and towards the cool end of the sample, where severe line blending and the increasing difficulty in the positioning of the continuum may also give rise to artificially high abundances. As a pertinent example, we mention the analyzed Moon spectra that exceed the expected solar abundance by ~ 0.02-0.03 dex. At present it is however not yet clear, whether this finding has its origins in the already mentioned problems with the spectrograph fiber, which particularly limits the quality of the available spectra, notably the exact positioning of the continuum. The next observing runs will hopefully give an answer to this question.

Another concern is related to the analysis of the Fe II lines: for the same reason that renders them very sensitive to the surface gravity parameter, they also respond to details of the relative elemental mixture, especially to the existence of an enhancement of α-elements in metal-poor stars. If not taken into account discrepancies of 0.1 dex are easily achieved. Consequently, many older analyses of metal-poor stars not only failed with the interpretation of Fe I lines for the reasons mentioned above, but also with the Fe II lines. Fortunately this disadvantageous behaviour of the Fe II lines is considerably relaxed for
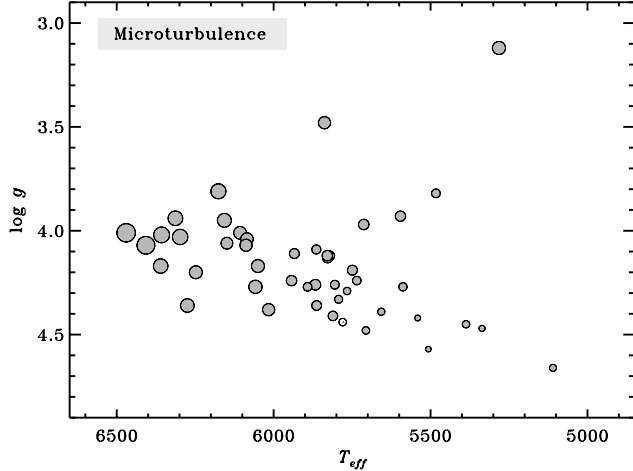
Fig. 5. The microturbulence dispersion of the program stars. Circle diameters are in proportion to the ξ_t values of Table 1. A smooth correlation along the main-sequence and towards evolved stars is noticeable. The dependence on metallicity is weak (cf. for instance the neighboring ρ^1 Cnc and μ Cas)

Fig. 7. Same as Fig. 6, but displayed in the T_{eff}-log g plane

the hotter stars, where the relative contribution of the hydrogen electrons is effectively increased in the line forming regions.

A final but no less important concern for the derived abundances has to do with the adopted microturbulence parameter, as discussed in the preceding section. Fig. 5 displays the results for our sample in the T_{eff}-log g plane, where it emerges as a smoothly variing function with only little response to the stellar metallicity. This uncomplicated behaviour argues against the occurrence of imponderable effects as a result of an otherwise poorly understood phenomenon; nevertheless errors in [Fe/H] on the 0.04 dex scale as a result of uncertainties in ξ_t cannot be excluded. Taking all these uncertainties into account, accuracies in metallicity better than Δ[Fe/H]=0.05 dex are presumably beyond the scope of our current abilities, irrespective of the possibility that errors in T_{eff} and log g may actually be very small.

If we compare the results of Fig. 5 for the microturbulence parameter with the findings of Gray (1984, 1992) for the related large-scale motion, it is no surprise that the ζ_{RT}/ξ_t ratio displayed in Figs. 6 and 7 is fairly well correlated and in particular very flat above $\sim$5500 K. Consequently, one might compute the macroturbulence parameter from a star's ξ_t value. On the base of our rather small sample this result is however at best preliminary and requires further confirmation.
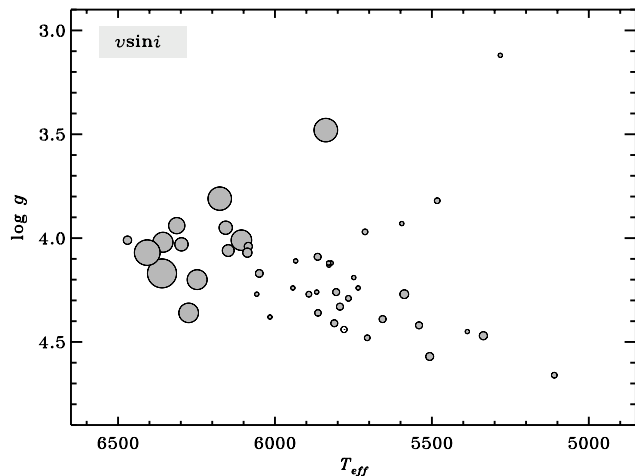
Fig. 8. Distribution of the projected rotational velocities. The diagram confirms the well-known finding of a marked onset to high $v\sin i$ values for F-type stars

Fig. 6. Correlation of the macro-/microturbulence ratio vs effective temperature

Another interesting and also much-discussed characteristic is the overall distribution of the projected rotational velocities displayed in Fig. 8. The rapid decline towards slow rotators for late-type stars is generally assumed to be the result of a convectively induced magnetic-dynamo braking. Our data imply a hot end for a successful spindown slightly below $T_{eff} \sim 6100$ K

the sample is not that large as to draw firm conclusions, and should consult a detailed discussion of the stellar ages as well.

The stellar radii presented in Fig. 9 are immediately obtained from the stars' luminosities and effective temperatures. The error estimates tabulated in column (15) of Table 1 assume the quadratic addition of the individual uncertainties. Interestingly, most stellar radii turn out to be fixed to better than 5%, a result that of course benefits very much from the accuracy of the Hipparcos parallaxes. If, as argued above, the Balmer lines provide a fairly well-defined effective temperature scale, the given stellar radii may indeed be very reliable. A tiny systematic effect is nevertheless conceivable from the adopted bolometric corrections in column (13): an increase of the tabulated values by $\Delta BC_V = 0.05$ mag, entails a $\sim 2.3\%$ decrease of the stellar radii. For comparison, increasing the effective temperatures by $\Delta T_{eff} = 50$ K corresponds to a $\sim 1.7\%$ decrease in radius.
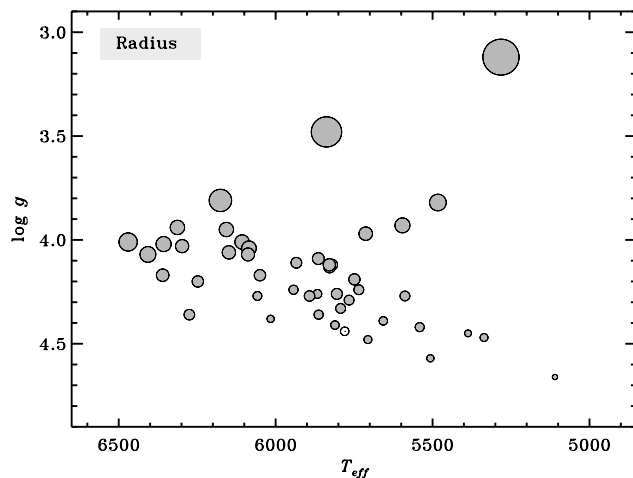
Fig. 9. Distribution of the stellar radii

For a comparison of the spectroscopically deduced parallaxes with the astrometric scale some information of the stellar masses is required and usually obtained from evolutionary tracks. If however we make use of T_{eff}-M_{bol} diagrams, instead of T_{eff}-log g *Kiel diagrams*, this is admittedly a small inconsistency, in that the derived masses are not obtained on purely spectroscopic grounds. But since our primary interest is to investigate the reliability of the surface gravity parameter and Hipparcos provides solid data for the M_{bol}'s of nearby stars, we preferred to decouple the mass and log g determinations. A posteriori it is however clear that the spectroscopic gravities indeed imply almost exactly the same stellar masses from the T_{eff}-log g diagram.

Our stellar mass estimates are tabulated in column (14) of Table 1 and displayed in Fig. 10. We repeat the above mentioned concern that they may have general uncertainties of up to 10% and many of them are probably subject to additional small adjustments on the base of forthcoming computations.

sults of Fig. 3: a systematic 5% increase of the stellar masses increases the spectroscopic distance scale by $\sim 2.5\%$.
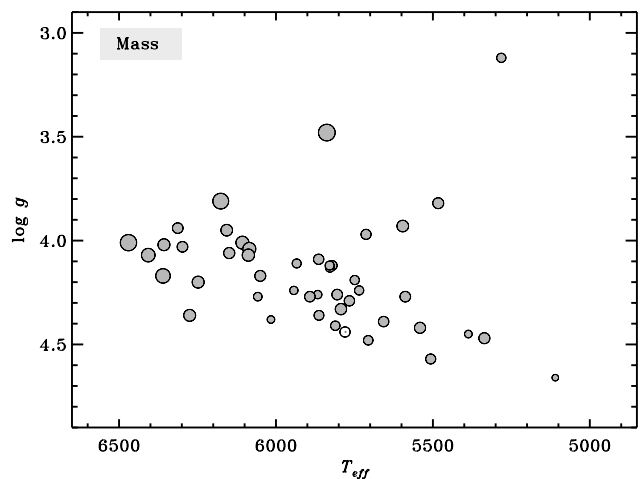
Fig. 10. Distribution of the stellar masses

A very important parameter for Galactic evolution studies is the relative [Mg/Fe] abundance as a function of a star's overall iron abundance and age that is shown in the upper panel of Fig. 11. Here the circle diameters are meant in proportion to the stellar ages. Though many of them are at present only qualitative estimates, a few basic results are nevertheless indicated to an interesting accuracy (a detailed discussion of refined stellar age determinations will be given in due course).

In what follows we shall procede however with the perspective displayed in the lower panel of Fig. 11 that gives an improved understanding in terms of sites of nucleosynthesis, with magnesium, being a principal SN II product, as the independent variable and [Fe/Mg] as ordinate. Notably this point of view reveals a remarkable feature, in that the α-enhancement – or, more precise, the *iron deficiency* – can be found in stars up to solar magnesium abundances, where a distinct *edge* occurs. On the other hand, most of the magnesium-rich stars tightly follow the *solar* Fe/Mg abundance ratio.

With a sample of less than fifty stars there is again a certain danger for an overinterpretation of Fig. 11, but nevertheless the scatter in terms of [Fe/Mg] among the old magnesium-poor stars suggests a lower degree of mixing of the corresponding protostellar material[1], as opposed to the objects with [Mg/H]>0 that show a well-defined relative solar abundance mixture. Hence, there is evidence from chemistry for what we usually call a *stellar population* and notably the stars at approximately solar Fe/Mg abundance are immediately recognizable as the *thin-disk* component. The abrupt change at [Fe/Mg]=−0.4 and solar magnesium abundance, with a paucity of old stars on the way "up" to solar abundance ratios, on the other hand, is very indicative

---

[1]   in this connection we also refer to the results of recently analyzed halo stars by Nissen & Schuster (1997) and King (1997)
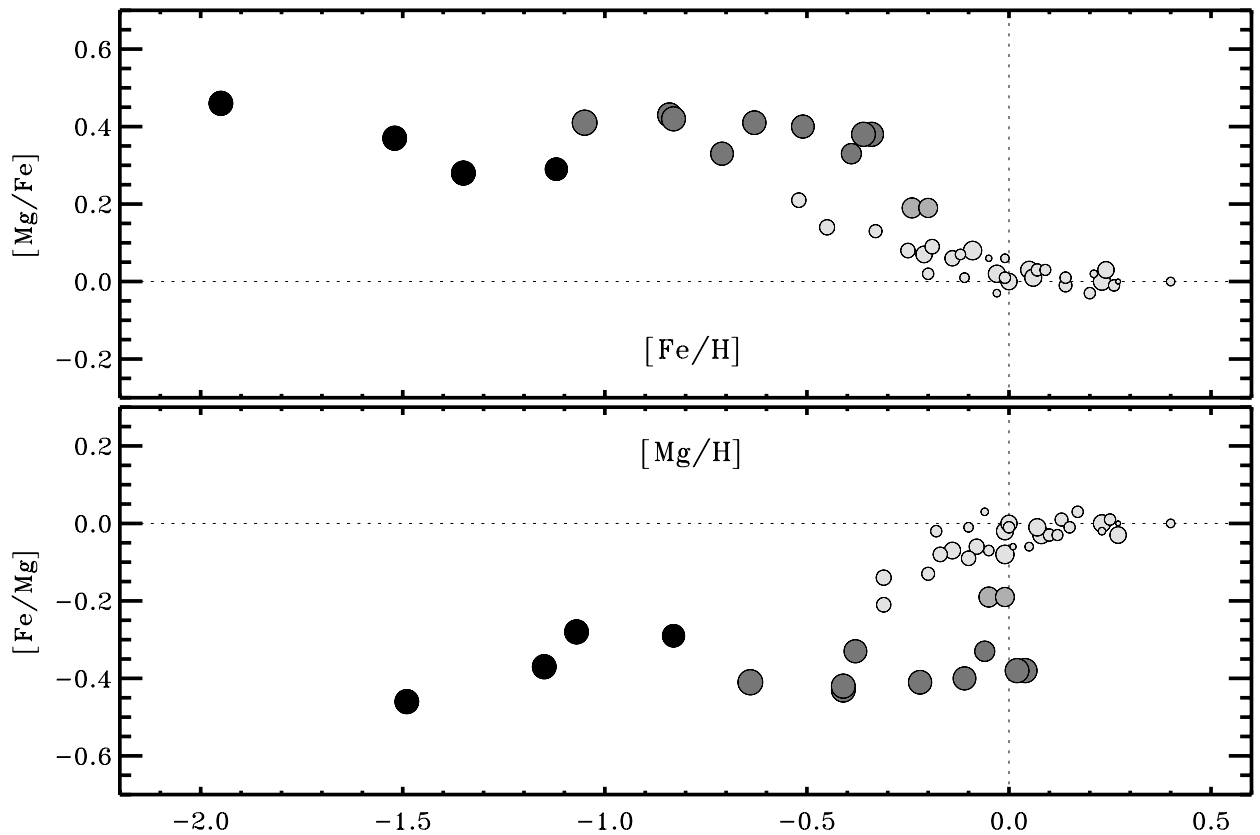
Fig. 11. Top: abundance ratio [Mg/Fe] vs [Fe/H]. Bottom: the same data, but with magnesium as reference element. Circle diameters denote age estimates, with small diameters indicating the youngest stars. Different *stellar populations* are given with various grayscale symbols as indicated in the legend on top, and are based on abundance, kinematics and age informations (see text for details)

of an epoch, where the early Mg enrichment from SN II events had come to an end and was followed by a gradual SN Ia-driven build-up of iron, while the star formation rate was at a minimum. The next phase of activity, which we identify with *the onset of the Galactic thin-disk formation*, then led to very high magnesium abundances which were the seeds for many long-lived stars formed right from the start: age determinations of magnesium-rich thin-disk stars like 16 Cyg, HR 7670, μ Her and 70 Vir provide very strong evidence that at least $\sim$8-9 Gyr elapsed since then, whereas both, ρ CrB and HR 7569, in the transition region at [Fe/Mg]= -0.2 must be very close to $\sim$10 Gyr (J. Bernkopf, private communication). As opposed to this, it appears that those stars with [Fe/Mg]< -0.25 are at least that old (HD 165401) or even well above 12 Gyr.

The fact that some stars on the high side of Fig. 11 do have considerable ages supports the notion of a weak age-metallicity relation for the thin disk for at least the above mentioned past $\sim$8-9 Gyr. Similarly, the iron deficient turnoff stars 72 Her and HD 221830 surpass the solar magnesium abundance, although they may be as old as $\sim$14 Gyr. Therefore, Fig. 11 is not a

simple evolutionary sequence in the sense "from left to right", but instead, the fairly well-defined sequence of metal-rich stars with almost zero slope in the relative elemental mixture, as well as the general iron deficiency ([Fe/Mg]< -0.25) among the old ($\geq$10 Gyr) stars, provide a clear signature that Fig. 11 is predominantly a *stellar population diagram*.

We have indicated this finding by means of different grayscale symbols as explained in the legend on top of Fig. 11. The *halo* component is separated by the dividing line presented in the [Fe/H]-V_{rot} diagram of Schuster, Parrao & Contreras Martínez (1993) that combines the stellar velocity component in the direction of the Galactic rotation, with the stars' metallicities. Thereby HD 184499, HD 201891 and μ Cas are close to the limit of the halo stars, whereas HD 194598 is already identified as such (the exact assignment is however of only minor importance in this context, since we are rather concerned with the separation of the two disk populations). The stars with solar [Fe/Mg] metallicities, on the other hand, must be the usual *thin-disk* stars, as explained above, but one may realize that there is also an elongated tail in Fig. 11 to

overlap in metallicity with the old, iron-deficient stars, they cannot be confused with this component on the base of their age and kinematics: the four most "extreme" of these, 15 Peg, HR 1545, 36 Dra and HR 17, are presumably younger than $\sim$7 Gyr and show V_{rot} values typical for thin-disk stars, whereas those denoted as the *thick-disk* component in Fig. 11 possess an asymmetric Strömberg drift of $\sim$70 km s^{-1}. This, at first glance, considerable lag in rotational velocity may have to do with the relative small sample involved, but the good separability of the thin- and thick-disk stars in the [Mg/H]-[Fe/Mg] plane of Fig. 11 certainly has a non-negligible impact as well. Note in particular than an adequate segregation of samples selected on grounds of high proper motion and flagged with a single metallicity parameter cannot be achieved. The presence of disk stars as old as the Sun, but borne in metal depleted (both in Mg and Fe) surroundings, is again indicative of a rather insignificant age-metallicity relation for the thin-disk population and the notion that chemical enrichment does not proceed in a straight and regular manner.

We recall that with our small sample of stars part of the interpretation of Fig. 11 must be preliminary at present, but nevertheless there can be no doubt that diagrams of this kind which combine metallicity, elemental abundance ratios, kinematics and age provide *first class* information on the ancient epochs, on stellar populations, the chemical evolution, and the process of galaxy formation in general. We return to this point in the final section.

4.2. Spectroscopic binaries

Even if we would have tried not to pollute the sample with spectroscopic binaries, in practice this hope is almost never fulfilled. In case of double-lined spectroscopic binaries the diagnostics of the combined light can actually be trivial and straightforward. Unresolved stars of very similar spectral types, on the contrary, may put the interpretation in a false light with almost no chance of detection. In between there is imaginably a *continuum* of possible outcomes. Some stars reveal suspicious broad lines for their spectral types, whereas others show up strange looking wings of strong lines. These cases could reliably be discarded, but there are also other objects that appeared to be not at all unusual, until we compared the spectroscopically deduced parallaxes with the Hipparcos astrometry. As an illustrative example of how the determination of the effective temperture can be affected, we show in Fig. 12 the combined Hα line of two main-sequence stars at T_{eff} = 5000 K and 6000 K. The putative single star receives $T_{eff} \sim$ 5700 K. The assumed zero Doppler displacement makes it particularly difficult to detect meaningful anomalies in the line wings, and it is clear that spectroscopic analyses like this must be erroneous right from the start.

As displayed in Fig. 3 our spectroscopically deduced distances have a small systematic offset of 3.4% on average, but, most remarkable, the corresponding *rms* error is also well confined to 5%. Therefore, the comparison of the spectroscopic
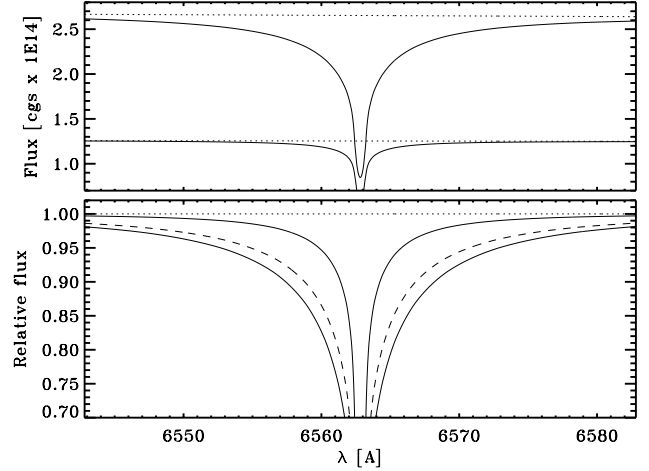
Fig. 12. Hα line profiles for two solar main-sequence stars with fixed log g = 4.50 and for T_{eff} = 5000 K and 6000 K. Top: absolute profiles; bottom: normalized profiles, with the dashed curve as the combination of both, assuming zero Doppler displacement. An effective temperature $\sim$ 5700 K is indicated for the spectroscopic binary

distances with the Hipparcos distances enables an identification of spectroscopic binaries or other "anomalous" stars on statistical grounds by means of e.g. an iterative 3σ criterion.

In this respect three stars were immediately identified as outliers and are depicted by open circles in Fig. 3. Two of them are in fact known spectroscopic binaries, although we were not aware of Carney et al.'s (1994) detection of G 78–1 at the time of observation. The very large discrepancy, however, made this object an almost certain case. ϵ Lib, identified at 4.24σ, has a known orbit with a period of 226 days (cf. Jones 1931, Abt & Levy 1976). 79 Cet (4.11σ) is – to our knowledge – not known as a binary, but from the results of Fig. 3 we suspect it as such.

There are three other stars in Fig. 3 depicted by open circles, although they do not meet a rigorous 3σ criterion: γ Ser and 35 Dra will be briefly discussed in the next subsection, whereas 99 Her is a well-known visual binary that we intentionally included in the sample for this system provides a rather well-defined *laboratory* with two components that are currently separated by only a few tenths of an arcsec (cf. Eggen 1965, p.26, Ghez et al. 1995, Heintz 1996). Compared to the seeing conditions of our observations, which were $\sim$ 2."5, this means that the light of both stars was superimposed on the detector.

The 99 Her system has been tracked since more than a century (cf. Kamper & Beardsley 1986), the orbital period is about $\sim$56 years. The A component at V=5.05 is classified as F7V, the B component at V=8.45 as K5V. Our analysis of the combined light results in T_{eff} = 5994 K, log g = 4.01 and [Fe/H]= -0.61. In comparison with the work of Edvardsson et al. (1993), who derive log g = 4.48, this is a huge discrepancy for the log g parameter that is not observed for any other common object (cf. Fig. 15 below). With respect to the Hipparcos data our spectroscopically inferred distance deviates by 16.2% which corresponds to 2.60σ. Hence, on grounds of only this

troscopic binary. In fact, Fig. 12 implies that the A component may actually be somewhat hotter than our derived T_{eff} value and this entails adoption of a slightly higher mass than given in Table 1. An ~ 0.2 dex higher value for the surface gravity would then be required to coincide with the Hipparcos distance scale.

In summary, we may learn from the 99 Her *experiment* that the Δm=3.4 mag difference is most likely *no* guarantee for an unbiased analysis. Although the status as a visual binary allows for an independent information of the primary's V magnitude, we find discrepancies with the astrometric distance scale as a result of wrong stellar parameters, notably the log g. More distant spectroscopic binaries will bring the *combined V* magnitude as an additional parameter of uncertainty into play and thereby augment the various manifestations of multiplicity in terms of spectroscopically inferred distances.

4.3. Notes on individual stars

In this subsection we comment on some spectroscopic binaries or suspected candidates, as well as few other stars of particular interest.

44 And: according to Fig. 8, there is some doubt about the reality of the derived high $v\sin i$ value. 44 And is also clearly discrepant in comparison with the log g derived by Edvardsson et al. (1993, see Fig. 15 below) which is somewhat reminiscent of 99 Her in the preceding subsection.

On the other hand, Beavers & Eitter (1986) and Duquennoy & Mayor (1991) report a constant radial velocity, and there is evidence for the correctness of the high $v\sin i$(11.6 km s^{-1}) from the the rotational modulation of the Ca II lines (Baliunas et al. 1983, 1985) and from the Ca II activity-rotation relation (Noyes et al. 1984) which imply a rotation rate of about two weeks; with $R_\star = 3.58\ R_\odot$ this results in an equatorial velocity $v \sim 13$ km s^{-1}. Note also that 44 And is thought be somehow related to the stars of the Ursa Major Group ($\tau \sim 0.3$ Gyr), although a certain membership has been questioned by Soderblom & Mayor (1993).

HD 45282: this is the only star in the sample with a significant parallax error $\sigma_\pi/\pi = 0.13$ that could give rise to an underestimated astrometric distance of $\sim 6\%$. All other stars have uncertainties $\sigma_\pi/\pi < 0.06$ and require negligible statistical corrections.

HR 5534: the somewhat peculiar appearance of the Mg Ib lines prohibits a meaningful log g determination. In addition, the projected rotational velocity, $v\sin i \sim 7$ km s^{-1}, appears to be too high for the star's position in the *Kiel diagram* of Fig. 8 with $T_{eff} \sim 5940$ K, and in view of the fact that the star may be as old as the Sun according to $M_{bol} = 4.47 \pm 0.06$ and [Fe/H]~ 0.0.

Since HR 5534 is known to be chromospherically active (e.g. Strassmeier et al. 1990), with a filled-in Hα core and emission line core-reversals in the Ca II H and K lines, and since binary stars show generally higher levels of activity than single stars, one may conjecture that HR 5534 is most likely

could then be considerably hotter, and thereby explain the observed high $v\sin i$. Although this would cause the star to be also much younger, which could favourably account for the observed level of chromospheric activity, this argument is of course self-defeating if put forward *against* the existence of a companion.

γ Ser: this star deviates by almost 3σ in Fig. 3. The line profile analysis reveals a considerable projected rotational velocity ($v\sin i = 10.6$ km s^{-1}), that is, a pole-on perspective that would hamper the detection of stellar radial velocity variabilities is less probable. Hence, with the reasonable assumption of a rather high inclination angle the absence of periodic Doppler shifts in the analyses of Abt & Levy (1976) as well as Duquennoy & Mayor (1991) argues against a putative companion. Along with the star's nearness (11 pc) the usual claim of binarity is therefore perhaps not very convincing.

As an explanation to the prevailing discrepancy we note instead that γ Ser is also known as a *variable* star. Recent confirmation of this finding is given in Cochran & Hatzes (1994) and Butler et al. (1997). Both works also report on the existence of a high level of intrinsic variability for some additional mid-F (F5-F7) dwarf stars. Cochran & Hatzes, in particular, conjecture *"... that these stars may represent the extreme tail end of the cool δ Scuti stars, or they may be a new class of variable stars in their own right ..."*. Thus, it may well be that our standard model atmosphere treatment cannot cope with this kind of activity. In this case, other stars (τ Boo, ι Psc, 35 Dra) in γ Ser's vicinity in the *Kiel diagram* of Fig. 2 might be affected as well. Note however that this may also depend on metallicity and/or age of the stars, and the time of observation, since, according to Butler et al. (1997), erratic fluctuations during timescales of years are followed by relative quiescence on similar timescales.

35 Dra: the data of Fig. 3 show a 2.64σ discrepancy, which causes some doubt on the assumption of a single object. Although Abt & Levy (1976) report a constant radial velocity, this is not necessarily in contradiction to the data of Fig. 8 and Table 1 ($v\sin i = 2$ km s^{-1}) that imply a rather low inclination angle for 35 Dra. Thus, we suspect the star to be either a spectroscopic binary, or, in analogy to γ Ser, characterized by some kind of activity.

HR 7955: is a double-lined spectroscopic binary; see also Anderson & Kraft (1972).

HD 201889: this star could not be analyzed for its strange appearance of the Mg Ib line wings. To the blue of this triplet the bunch of molecular features is typical for a K- or late G-type star and disagrees with the findings from the Balmer line wings that favour an effective temperature close to ~ 5770 K. The suggested presence of a binary is also confirmed by the results of the Hipparcos data, that tabulate two stars at an angular separation of 1.429 arcsec and a magnitude difference of 2.03 mag.

HD 201891: this is an often referred metal-poor standard, but interestingly, there is considerable confusion in the literature with respect to all three basic spectroscopic parameters.

ity [Fe/H]= -1.42, a value that has entered many analyses, e.g. the recent review by VandenBerg, Bolte & Stetson (1996). As opposed to this, our results imply [Fe/H]= -1.05, which deviates by more than a factor of two, but is also confirmed by Edvardsson et al. (1993). With respect to the surface gravity the latter work implies $\log g = 4.46$, which agrees with Carney's $\log g = 4.50$, but, as has recently been shown by Nissen, Høg & Schuster (1997), disagrees with the Hipparcos astrometry that fixes the $\log g$ close to ~ 4.25. Nissen, Høg & Schuster however derive $T_{eff} = 5800$ K, which, although confirmed by Carney's analysis, is in conflict with the isochrones of Bergbusch & VandenBerg (1992). For this reason they suspect HD 201891 to be a binary. This is also "... the most plausible explanation ..." according to Pont et al. (1998).

With our ~ 140 K higher effective temperature obtained from the Balmer line wings there is nothing unusual with this star, which is currently ascending to its turnoff position in the HR diagram.

HD 210277: there is some contradicting information on the spectral type and luminosity class of this star in the literature. This may be explained by the finding that it is actually a super-metal-rich object, i.e. heavily line-blanketed. The surface gravity is found to be very close to the solar value, and preliminary evolutionary tracks (J. Bernkopf, private communication) are suggestive of an age comparable to the Sun.

ι *Psc*: there is the possibility of binarity according to Duquennoy & Mayor (1991), but see also Murdoch, Hearnshaw & Clark (1993) and Heintz (1993). The reader is also referred to the above given comments on γ Ser, should this star be variable in a similar manner.

4.4. Comparison with related analyses

As in Sect. 4.1, we first compare the Hipparcos data with some photometric/spectroscopic distance scales, namely Hearnshaw (1972, 1974a,b,1976), Edvardsson et al. (1993), Carney et al. (1994) and Gratton, Carretta & Castelli (1996). Except for Carney et al., who do not derive explicit surface gravities, we prefer to calculate the stellar distances by means of the published T_{eff}, $\log g$ and [Fe/H] values (note that Edvardsson et al. provide a photometric distance scale as well). This is, because we are chiefly interested in a comparison of the basic atmospheric parameters, in particular the surface gravity. In calculating the photometric/spectroscopic distances we make use of the same V magnitudes, the same tables of bolometric corrections given by Alonso, Arribas & Martínez-Roger (1995), and, albeit slightly incorrect, adopt our mass estimates from column (14) of Table 1 for convenience and because this is no real concern for the comparison of the distance scales.

In Fig. 13 the resulting data are presented in the same manner as in Fig. 3, although those stars that were already found to be discrepant are not included. By application of analogous 3σ criteria we can see that Hearnshaw's data suggest another discrepant star (HR 4550), whereas Edvardsson et al. provide two such objects: 44 And (3.89σ) and 51 Peg (3.72σ).

yses we now proceed with a more detailed discussion of the individual stellar parameters.

Hearnshaw (1972, 1974a,b, 1976)

The main shortcomings of this work are certainly both, theoretical and observational, since our abilities have significantly improved within the last two decades. But in view of this, the accuracy achieved by Hearnshaw is on the contrary quite remarkable, with only few outstanding analysis errors, such as the derived surface gravity value for HR 4550 (cf. Fig. 14).
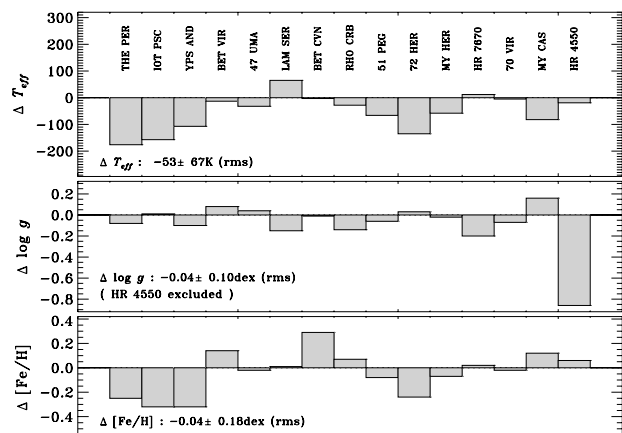

Fig. 14. Comparison of the basic spectroscopic parameters T_{eff}, $\log g$ and [Fe/H] for stars in common with Hearnshaw (1972, 1974a,b, 1976), in the sense "Hearnshaw *minus* this work", and for decreasing effective temperatures (left to right). There is a *shift* towards *lower* temperatures in Hearnshaw's analyses

Edvardsson et al. (1993)

This analysis deals with 189 nearby F- and G-stars, most of which are in slightly evolved stages of evolution to enhance the accuracy of the stellar age determinations. The effective temperatures and surface gravities are derived from Strömgren photometry. The abundance analysis is based on high resolution, high S/N spectroscopic observations. As displayed in Fig. 13 this work shows the comparatively best results with respect to the astrometric distance scale. Details of ΔT_{eff}, $\Delta \log g$ and Δ[Fe/H] for common stars are shown in Fig. 15. As is most obvious, there is a slope in the ΔT_{eff} values from hot (left) to cool (right) stars, but only small systematic shifts to higher $\log g$ values and lower metallicities.

With respect to the effective temperature scale, the largest deviation in Fig. 15 occurs for the hottest star, the F5 standard *Procyon*. Edvardsson et al. tabulate $T_{eff} = 6704$ K which contrasts with our value $T_{eff} = 6470$ K. Direct stellar diameter and flux measurements are however known to yield values
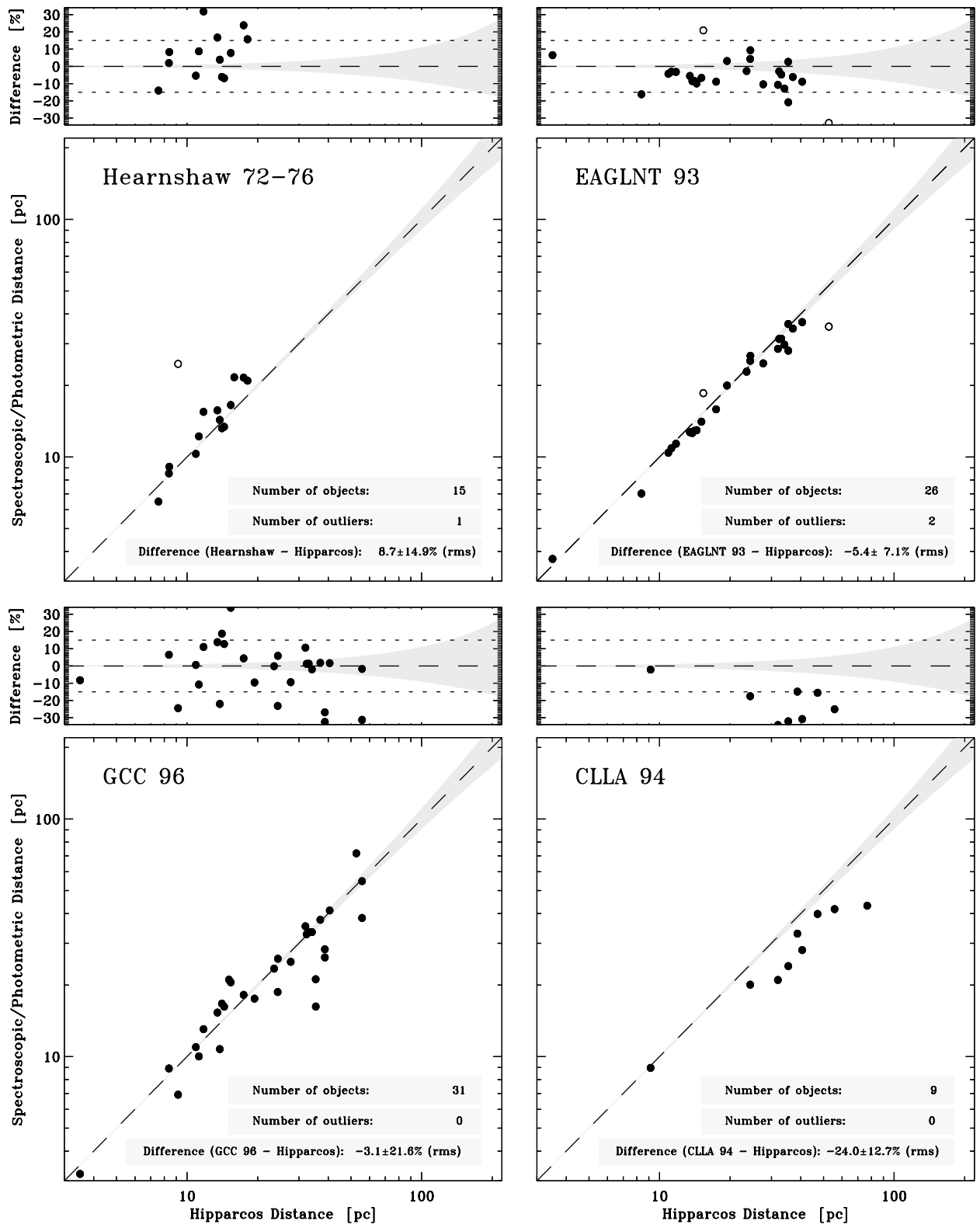
Fig. 13. Same as Fig. 3, but for stars in common with the work of Hearnshaw (1972, 1974a,b, 1976), Edvardsson et al. (1993, "EAGLNT93"), Gratton, Carretta & Castelli (1996, "GCC96"), and Carney et al. (1994, "CLLA94")
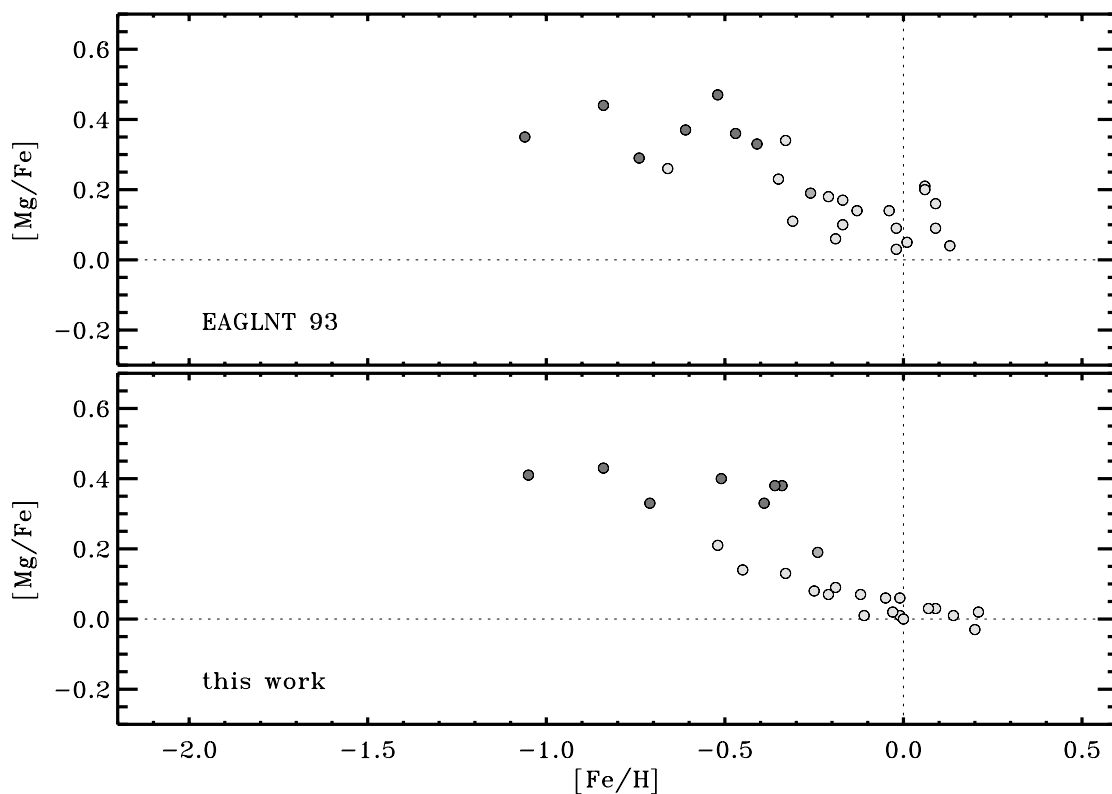
Fig. 16. Comparison of the [Mg/Fe] abundance ratio for stars in common with the work of Edvardsson et al. (1993) and the same grayscaling as in Fig. 11
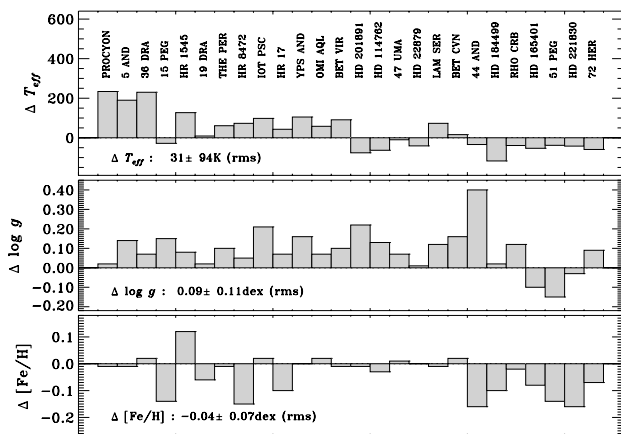

Fig. 15. Same as Fig. 14, but for the work of Edvardsson et al. (1993). The comparison reveals a deviating *slope* for the effective temperature scale, as well as small shifts towards *higher* surface gravities and *lower* metal abundances

close to 6500 K. In this connection it is important to note that Edvardsson et al. make use of Fe I lines for their metallicity scale. As already discussed in the preceding sections, this species is a rather doubtful choice for F stars. Lowering the

effective temperature value for *Procyon* by 200 K could easily result in a corresponding decrease in metallicity by ~ 0.15 dex. That is, although both metallicity scales for this star are in almost perfect agreement in Fig. 15, this is a result of the deviating effective temperatures, or vice versa, if both T_{eff} scales would agree, there would be a significant discrepancy in metallicity.

If however the effective temperature of *Procyon* is indeed close to 6500 K, and other stars in this temperature range – as indicated in Fig. 15 – do reveal similar discrepancies, this implies that a good deal of the results for the hotter stars in Edvardsson et al. are subject to systematic errors, in particular the age determinations.

Another aspect that reveals the limited accuracy of the published magnesium-over-iron abundance values in Edvardsson et al. is displayed in Fig. 16. As is immediately obvious, most of the scatter in the data of Edvardsson et al. vanishes in the lower panel, where exactly the same stars, but with the data of the present analysis, are repeated. A detailed interpretation, like we have done in Fig. 11, is evidently prohibited on the base of the data in the upper panel. Nevertheless, we should mention that at least the kinematical aspect of the relevant discussion in Fig. 11, i.e. an abrupt change about 10 Gyr ago is also obtained by Edvardsson et al. (cf. their Fig. 16) and also discussed in more detail by Nissen (1995).

The authors investigate about 300 stars in a homogeneous way by means of photometric indices, like $V - K$, for the effective temperatures, and Fe I and Fe II lines for the surface gravities and metal abundances. Most of the equivalent width measurements are published literature data, the majority from the large data base of Edvardsson et al. (1993). As a result, all of the stars in Fig. 15 are also represented in Fig. 17.
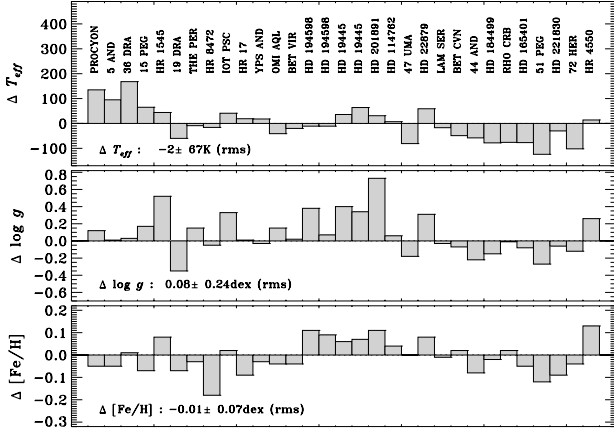
Fig. 17. Same as Fig. 14, but for the work of Gratton, Carretta & Castelli (1996). There is a similar *slope* of the effective temperature scale as in Edvardsson et al. (1993), as well as significant *scatter* for the surface gravities. Note that a few objects appear twice in that work and consequently also in this figure
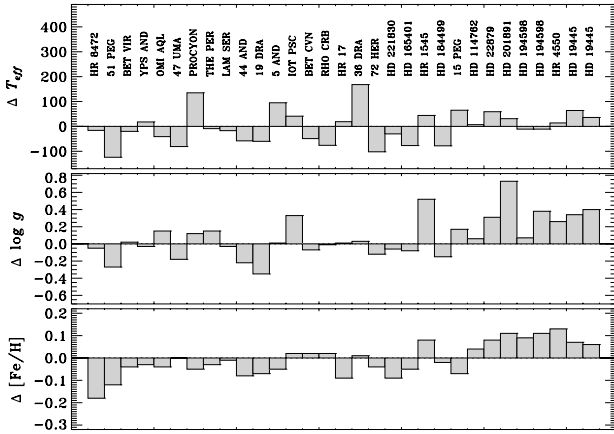
Fig. 18. Same as Fig. 17, but sorted along the metallicity scale. In this case we notice the strongest discrepancies in log g for the *metal-poor* stars, as well as a deviating *slope* in [Fe/H] in the bottom panel

reveals a similar deviating slope of the effective temperature scale, that is, as in Edvardsson et al., the F stars receive higher T_{eff}'s which causes Fe I and Fe II lines to result in similar abundances (as opposed to our findings of Fig. 4). With respect to the surface gravities we notice a similar offset as in Fig. 15, but with a more than two times enhanced scatter. As an explanation for this, we repeat the data in Fig. 18 now sorted according to the stars' metallicities, which reveals the largest discrepancies to occur for the metal-poor stars. The comparison of our [Fe/H] values with those of Gratton, Carretta & Castelli shows a very good agreement in the bottom panel of Fig. 17; but from the perspective of Fig. 18 a slightly deviating slope is present.

Carney, Latham, Laird & Aguilar (1994)

In this study of a large sample of 1464 field stars selected from proper motion catalogues, photometric (distances and effective temperatures) and spectroscopic means (metallicities) are employed to investigate the local metal-poor populations. We do have only nine stars in common with Carney et al., but from the lower right panel in Fig. 13, which is a direct comparison of the Hipparcos parallaxes with their proposed photometric distance scale, it is clear that they have underestimated the stars' distances. This may have to do with the assumed dwarf stage for the program stars by Carney et al., unless independent evidence to the contrary was noticed. With the availability of the Hipparcos data, comparisons like Fig. 13 have already been done for much larger subsets (which is beyond the scope of our analysis) and we refer to Jahreiß, Fuchs & Wielen (1997) for a more detailed discussion in this connection.

Here we proceed with the results of the derived effective temperatures and metallicities for the few common stars in Fig. 19. The comparison of the T_{eff} scales shows a remarkable small scatter of 37 K *rms*, but the absolute values differ by -135 K. This circumstance is perhaps best explained by the authors' allowance for *"... an uncertainty of at least 100 K, and perhaps even 200 K, in our temperature scale zero points ..."* and the caution to *"... the reader that, in general, our temperature scale might result in temperatures 100 K or more, too cool, especially for the more metal-rich stars ..."*. A good deal (if not all) of the discrepancies with the metallicity scales in the lower panel of Fig. 19, is, no doubt, coupled with the deviating T_{eff} scales.

Balachandran (1990)

The investigated sample consists of about 200 bright F stars, slightly evolved off the main-sequence, with particular emphasis on lithium abundances and mechanisms associated with its depletion. Both, T_{eff} and log g of the program stars are derived from Strömgren photometry, whereas the metallicities are found from Coudé spectroscopy of Fe I lines next to the Li I resonance doublet at 6707Å. A major drawback of the analysis may be found in the reference to T_{eff}-scaled Holweger/Müller models (Holweger & Müller 1974). This is because the sample
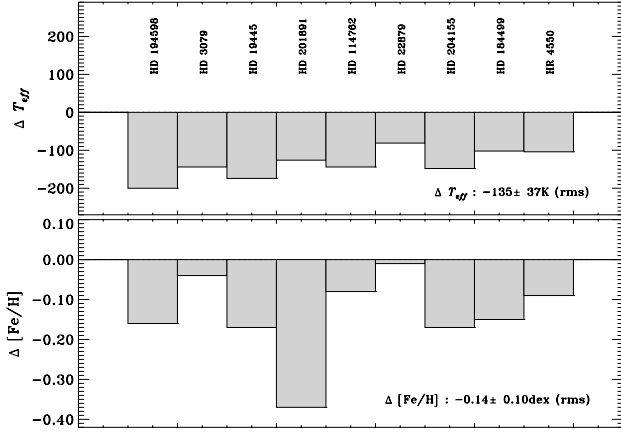
Fig. 19. Same as Fig. 14, but for the work of Carney et al. (1994). Both, the effective temperature and metallicity scales show offsets to *lower* values

stars are in the effective temperature range between 6000 K and 7000 K and it was shown by Steffen (1985, p.407) in his elaborate analysis of *Procyon* that a scaled Holweger/Müller model is not a good choice for this standard F star.

Although a similar comparison of the distance scale as in Fig. 13 shows a very small scatter of only 2.3% *rms*, the mean spectroscopic distance obtained from the stellar parameters deviates by -12.6%, i.e. the stars "become closer" than they actually are. The explanation for this finding is inferable from Fig. 20, as a corresponding offset in the surface gravity values that are too high in Balachandran's work. In addition, the mean difference of the iron abundances, as depicted in the bottom panel, amounts to approximately 0.1 dex.
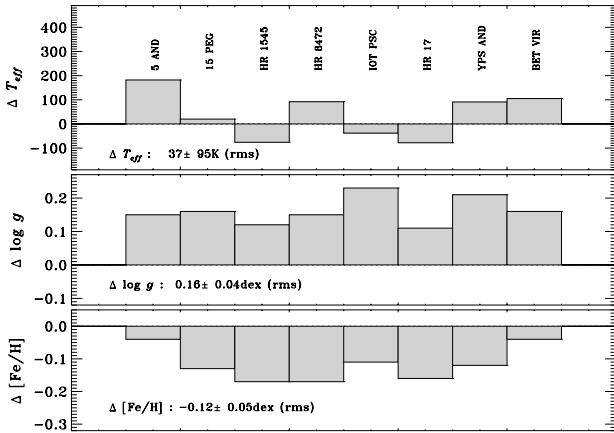
Fig. 20. Same as Fig. 14, but for the work of Balachandran (1990). The data are systematically shifted to *higher* surface gravities and *lower* iron abundances

This sample of ~700 metal-poor and high-proper-motion stars is analyzed by Strömgren $uvby - \beta$ photometry. The comparison of the metallicity scales in Fig. 21 shows a mean offset of -0.06 dex with no clear dependence on effective temperature. A repeated illustration, sorted according to metallicity, exhibits however all deviating stars to be metal-rich. The more metal-poor stars, in contradistinction, are in almost perfect agreement with our analysis.
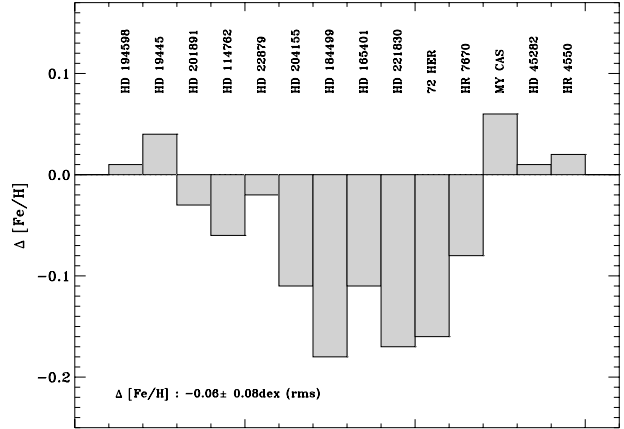
Fig. 21. Same as Fig. 14, but for the work of Schuster & Nissen (1988, 1989). Part of the stars shows *lower* metallicties by ~0.1 dex
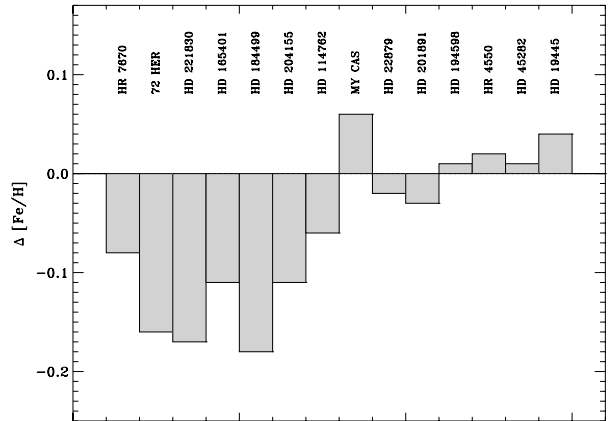
Fig. 22. Same as Fig. 21, but sorted along the metallicity scale. Evidently the discrepancies are confined to the metal-rich stars, most of which are associated with the thick disk in Fig. 11

Wyse & Gilmore (1995)

ity distribution of ~90 long-lived F- and G-dwarfs based on Strömgren photometry and the [Fe/H] calibration of Schuster & Nissen (1989). We do have only eight stars in common with that work, but from Fig. 23 it is evident that our results show somewhat higher metallicities. Closer inspection of Fig. 23 identifies the two metal-poor thick-disk objects, HD 22879 and HD 165401, to show consistent results with our metallicity scale. Hence, it appears that it is the thin-disk metallicity distribution of Wyse & Gilmore that requires a shift to *higher* abundances by ~0.1 dex.
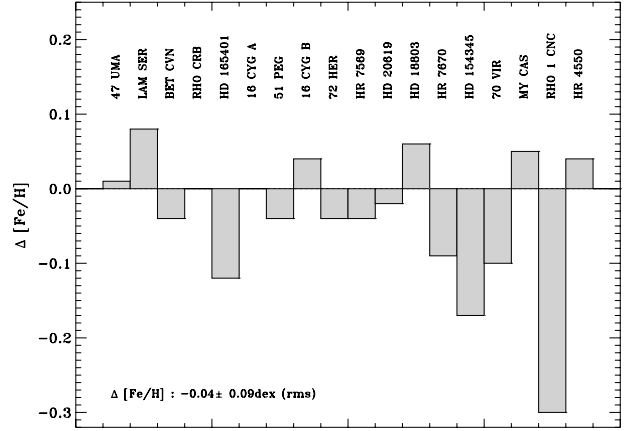

Fig. 24. Same as Fig. 14, but for the work of Rocha-Pinto & Maciel (1996). The metallicity scale is slightly displaced to *lower* values, with increasing dicrepancies towards lower effective temperatures for metal-rich stars

Fig. 23. Same as Fig. 14, but for the work of Wyse & Gilmore (1995), which shows systematically *lower* metallicities

Effective temperatures based on the infrared flux method are presented for 475 stars in this analysis. Most of stars are confined to $3500 \leq T_{eff} \leq 8000$ K and $-3.5 \leq$ [Fe/H]$\leq +0.5$. The comparison with our work for the about 20 common stars is shown in Fig. 25. Except for *Procyon*, the differences remain within 100 K, but there is a deviating slope that entails comparatively lower effective temperatures in Alonso, Arribas & Martínez-Roger for the cooler stars. A more detailed comparison of Fig. 25 reveals that this is largely ascribed to the thick-disk and halo stars: except for HD 19445, all ΔT_{eff}'s turn out to be negative, with a mean $\Delta T_{eff} = -64 \pm 19$ K (*rms*).

Rocha-Pinto & Maciel (1996)

Similar to the work of Wyse & Gilmore (1995) the authors reinvestigate the metallicity distribution of 287 solar neighborhood G dwarfs on the base of existing Strömgren photometry and by means of the same Schuster & Nissen (1989) metallicity estimators. As a result, it is no surprise that they find a similar maximum in the metallicity distribution some 0.2 dex below the solar abundance, as advocated by Wyse & Gilmore. Since Rocha-Pinto & Maciel provide a three times larger sample, we have accordingly more objects in common, displayed in Fig. 24. As with Fig. 23 for the comparison with the data of Wyse & Gilmore the *rms* scatter is nicely confined to 0.1 dex, and, in addition, the mean metallicity derived by Rocha-Pinto & Maciel deviates by only 0.04 dex. We note however a bias for increasing discrepancies toward cool, metal-rich stars. This again suggests that the peak in the corresponding metallicity distribution of nearby G dwarfs is presumably found at somewhat *higher* metallicities than implied from the Strömgren photometry.

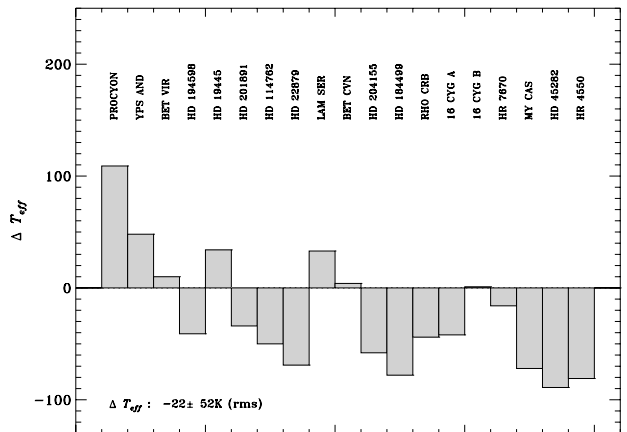### Alonso, Arribas & Martínez-Roger (1996)

Fig. 25. Same as Fig. 14, but for the work of Alonso, Arribas & Martínez-Roger (1996). There is a different *slope* in the effective temperature scale

In this work we addressed the impact of the basic stellar parameters of *nearby* field F- and G-stars for the understanding of the chemical and kinematical evolution of the Galaxy, the identification of distinct stellar populations, their potential interaction and possible origin. Spectra of about fifty such stars were analyzed on the base of standard LTE atmospheres and a detailed modeling of the profiles of many absorption lines. But irrespective of our differential approach, *direct* observations of some principal quantities – such as the stars' distances – are an invaluable help to scrutinize the reliability of the overall framework or at least part of it. The accurate Hipparcos parallaxes provide an important step in this direction, which the methods of spectroscopy must now withstand.

As was displayed in Fig. 3, this is actually achieved with the employed methods and results in a spectroscopic distance scale that is only slightly higher by 3.4% on average. In view of our assessment for the $\log g$ determinations to have a typical uncertainty of $\Delta \log g = 0.1$ dex – which translates to about three times the above distance error – this is indeed no real concern. On the contrary, it is quite remarkable that the spectroscopic distance scale shows a statistical *rms* error of only 5%. The potential of this favourable correlation with the Hipparcos data is convincingly demonstrated by its ability to identify several outliers as spectroscopic binaries.

But in spite of these encouraging results we should nevertheless keep in mind that the spectroscopic distance scale, though most susceptible to the surface gravity, is also dependent on other stellar parameters. In the preceding section we have already mentioned the stellar masses, where a 5% increase corresponds to a ~2.5% increase in distance. Similarly, a higher effective temperature scale by $\Delta T_{eff} = 80$ K results in a further ~3.4% increase of the spectroscopic distances, and higher values for the bolometric corrections by $\Delta BC_V = 0.05$ mag cause another increase of ~2.4%. Minor systematic analysis errors, for instance an erroneous placement of the continuum as a result of the unfavourable fiber noise, are also conceivable to have their share in the small distance discrepancy. If, as a result, the derived metallicities are slightly too high, this would have a small impact on the stellar masses. Another concern has to do with the LTE modeling discrepancies that we notice in the core region of the Mg Ib lines of especially metal-poor stars and which may affect the $\log g$ determination by a few hundredths of a dex.

We should also be aware that stellar variability (for some mid-F type stars) and undetected spectroscopic binaries may obscure the *offset* and *rms* accuracy of the spectroscopic distance scale. With respect to multiplicity it is important to recall that in spite of thousands of newly discovered binaries from Hipparcos, this *"... instrument was not ideally suited for the observation of resolved objects ..."* and *"... while most stars are in reality members of double or multiple systems, only a minority of these systems are manifestly non-single as seen by Hipparcos. Thus, 85 per cent of the entries in the Hipparcos Catalogue could in practice be treated as*

spectroscopic binaries, except for ϵ Lib, are found to the left of the 1:1 line. Similarly, ι Psc may be a spectroscopic binary as well. Note also that μ Cas is known as a spectroscopic binary (cf., e.g., Halliwell 1981, Duquennoy & Mayor 1991) and λ Ser is at least suspected as such (Abt & Levy 1976; but see Duquennoy & Mayor 1991 and Morbey & Griffin 1987 for a different point of view). Hence, the results of Fig. 3 may indeed be biased to some extent.

Finally, Fig. 4 reminds us that certain regions of the HR diagram are either very sensitive to NLTE effects of important species like Fe I, or the underlying model atmospheres are still subject to major deficiencies. Without doubt, part of the existing problems do cancel however as a result of our *differential methods*. Along with the *large spectral coverage* of the FOCES spectrograph, that provides a homogeneous data base, we regard these two issues to be the most important ones for the fairly well-defined atmospheric parameters presented in this work.

As a direct consequence of the small distance scale error in Fig. 3 it is evident that stars of similar spectral types, but distributed on Galactic scales, can receive accurately determined distances – once a photometric V magnitude and a high resolution, high S/N spectrum is available. Of course, the more we proceed into space the Achilles' heel of the method will be the interstellar extinction A_V that affects a star's V magnitude. Nevertheless a solid, spectroscopically defined, distance scale of selected Galactic globular clusters by means of the new generation of large telescopes is fairly well realizable. Even more, with the exciting potential of short-term light magnifications via *microlensing* events, the challenging spectroscopic study of solar-type Galactic *bulge* stars (cf. Lennon et al. 1996) is no longer out of reach.

It is also important to note that in combination with the expected ~10 μas accuracy level of the next generation of astrometry satellites (e.g. Perryman, Lindegren & Turon 1997) the independent information of the spectroscopic distance scale offers the very promising chance for a careful and three dimensional mapping of the *interstellar medium* on Galactic scales.

With respect to the various stellar populations that make up the Galaxy we have seen that the [Mg/H]-[Fe/Mg] plane combined with age and kinematical informations provides a very useful means to discern the thick disk from the thin disk. Interestingly, *all* of our thin-disk stars in Fig. 11 are found to be younger than ~8-9 Gyr, whereas the thick-disk stars appear to exceed 10 Gyr (or even 12 Gyr), and the two stars that interrelate both disk populations, ρ CrB and HR 7569, have an age close to 10 Gyr.

Should this result be confirmed by larger samples of this kind[2], it certainly has several important implications: first, al-

---

[2] we note in passing that two stars designated in the sample of Edvardsson et al. (1993) as "outstanding examples" in view of their old, metal-rich status (HR 5019: [Fe/H]= -0.03, [Fe/Mg]= -0.08, $\tau = 14$ Gyr; HR 7232: [Fe/H]= $+0.03$, [Fe/Mg]= -0.06, $\tau = 12$ Gyr), and which we would identify in Fig. 11 as thin-disk stars, are not significantly older than ~8-9 Gyr on the base of their bolometric magnitudes derived from the Hipparcos parallaxes
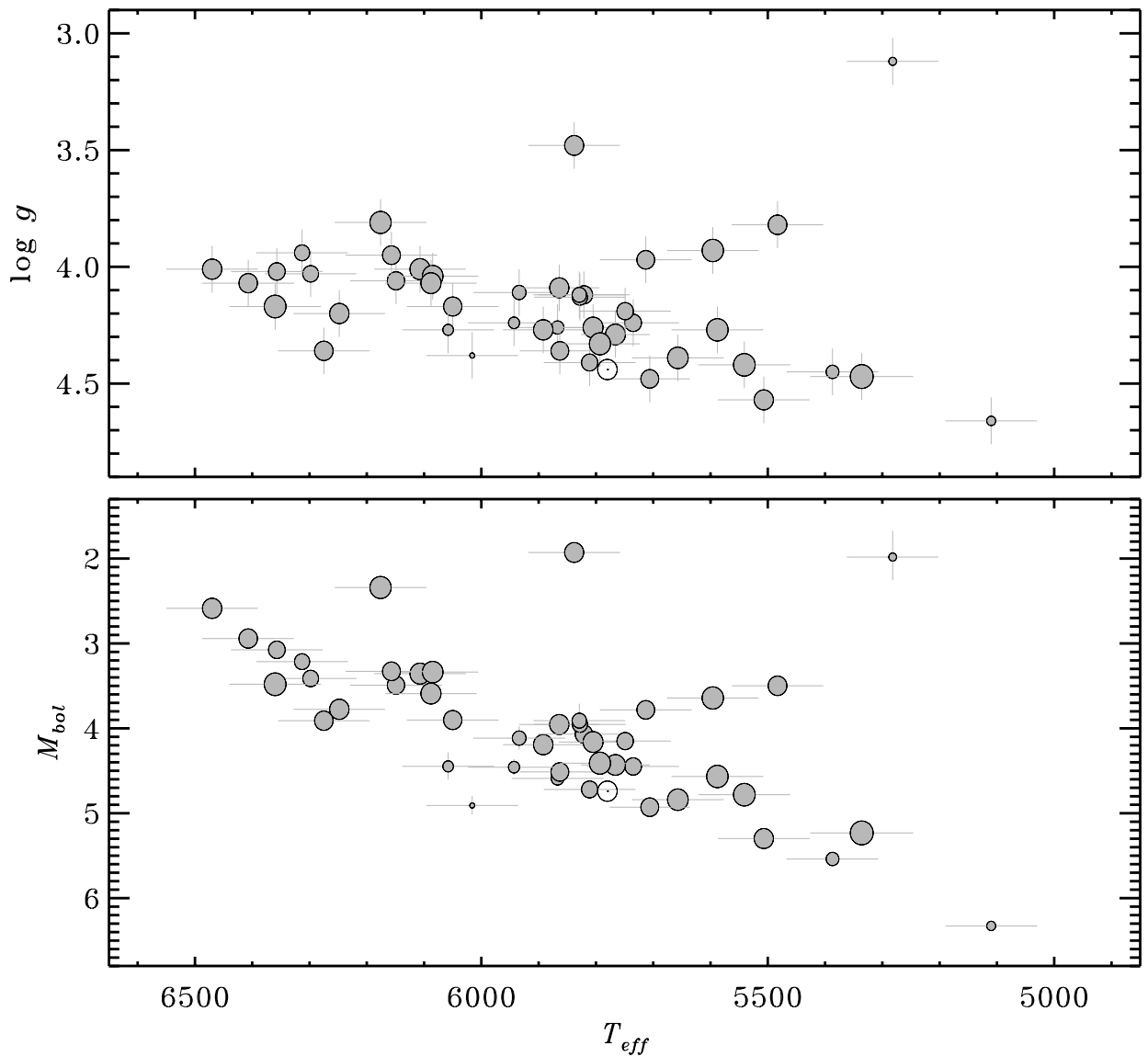
Fig. 26. Comparison of two physical HR diagrams. Top: the spectroscopic T_{eff}-log g *Kiel diagram* of Fig. 2 with error bars included; bottom: the analogous distribution in the T_{eff}-M_{bol} plane. Note that most stars show an almost negligible error in M_{bol} as a result of the solid Hipparcos astrometry. The upper *Kiel diagram*, on the contrary, has the advantage to be applicable to Galactic distance scales

though the thick disk itself may be a distinct merger population, a thin-disk heating scenario as envisaged by Quinn, Hernquist & Fullagar (1993) is of course very unlikely for a thick disk that is putatively older than the stars of the thin disk. Instead it seems that the thick disk is, in fact, the natural precursor of the thin disk (whether this happened from *top-to-bottom* or *inside-out*, as mentioned in the Introduction, is another question). Second, the abrupt change in [Fe/Mg] in Fig. 11 with relatively few stars along the upturn to solar Fe/Mg ratios, as well as the distinct kinematic behaviour of the thick-disk and thin-disk population, is suggestive of an intermediate phase characterized by contraction and spinup and a substantial release of iron-enriched

matter, but otherwise low or even ceased star formation. Third, the existence of old thin-disk stars with very high metal content argues in favour of an epoch of enhanced star formation at the onset of the Galactic thin disk. This is however not to be confused with a real *burst* that would impose a set-back in the evolution of the [Fe/Mg] values for the old Mg-rich thin-disk stars, which is not observed in Fig. 11. On the other hand, there are also no hints for stars with super-solar [Fe/Mg] values, as advocated by e.g. Edmunds et al. (1991), and more recently Chiappini, Matteucci & Gratton (1997), or as one might expect if the protostellar material of younger thin-disk stars is predominantly subject to delayed SN Ia events (cf., for instance, the

their Fig.10). This observational finding certainly constitutes a tight constraint to the relative occurrence and/or yields of SN I vs SN II events.

We note that part of these results is already discussed or present in the work of e.g. Edvardsson et al. (1993, cf. their Figs. 14 and 16b) and Nissen (1995), as well as Gratton & Carretta (1996) and Gratton et al. (1996). Thereby it seems that indeed there was a hiatus in star formation, before some $\sim$9-10 Gyr ago the earliest stages of the thin disk became evident.

In this connection the reader is also referred to the very intriguing discussion on a possible dichotomy in old open clusters that may belong to either the thin disk or the thick disk, with more thin-disk kinematics for those open clusters that have an age-dating $\leq$8 Gyr, whereas the two oldest, Be 17 ($\sim$12 Gyr) and NGC 6791 ($\sim$10 Gyr), show more eccentric orbits (cf. Majewski, Phelps & Rich 1997, and references therein).

Very recently, Ng & Bertelli (1998) have reanalyzed the stellar ages of the Edvardsson et al. (1993) sample on the base of revised isochrones and by inclusion of the Hipparcos parallaxes. Their Figs. 6 and 7 are again very indicative of the aforementioned star formation gap – on their scale between 10-12 Gyr. Although they summarize their results with the finding of a *"... small, but distinct slope of $\sim$0.07 dex/Gyr ..."* for the age-metallicity relation, a peek at their Figs. 6 and 7 from the perspective that two different stellar populations are involved is much more suggestive for a step-like metallicity increase at the thick-thin disk transition and *"... that there is no apparent age-metallicity relation for stars with an age less than 10 Gyr. We are basically dealing with a large metallicity spread among the stars ..."* which the authors mention in passing. Indeed, the displayed data of Ng & Bertelli (1998) endorse the view of a thin disk that came up with even super-metal-rich stars right in its early history. Again, this is not at variance with the existence of rather young and metal-depleted stars, as shown in Fig. 11, and as we can infer from the diagrams of Edvardsson et al. and Ng & Bertelli. Although it is likely that the onset of Galactic thin-disk formation was globally triggered, the chemical enrichment of matter most obviously is a process that involves a local dimension as well. In fact, as we can see from Fig. 11, and especially with reference to the [Mg/H] scale in the lower panel, the resulting metallicity distribution of the thin disk reaches well into the regime of the thick-disk stars, a finding that is also advocated by Wyse & Gilmore (1995) in their comparative study of long-lived solar neighborhood stars with two distant *in situ* samples.

For an alternative explanation to the existence of the metal-poor thin-disk stars one may however conjecture that the string-of-pearls-like distribution of these objects in Fig. 11 has to do with a *delayed infall* of processed thick-disk material that, while dissipational settling to the symmetry plane, underwent rotational spinup and gave rise to subsequent star formation. In this scenario, there is again no significant age-metallicity relation for the thin disk, but its more metal-poor stars result from rather lately accreted matter and are not primarily due to an insufficient mixing of the metal-rich debris of exploded supernovae.

putative age gap and considerable abundance overlap of the two disk components.

As a final item, we briefly discuss prospects of forthcoming Galactic globular cluster age-datings by means of a comparison of the two physical HR diagrams displayed in Fig. 26: the spectroscopic T_{eff}-log g *Kiel diagram* that was employed in many of the preceding figures, and the T_{eff}-M_{bol} diagram which is well-suited in combination with the accurate Hipparcos parallaxes. As is immediately obvious from the lower panel, the Hipparcos based bolometric magnitudes are that well determined to cause most of the corresponding error bars to become invisible from the depicted circle diameters. It is also most evident that both diagrams differ in many details (cf. again the neighboring ρ^1 Cnc and μ Cas) for the ordinate in the upper panel behaves as $\propto M R^{-2}$, whereas $M_{bol} \propto R^2 T_{eff}^4$. HD 45282, the most evolved star at the upper right edge in both diagrams, is situated at a distance of $\sim$137 pc, where the spectroscopically determined values become as accurate as the Hipparcos data. But as mentioned above, $\sim$100-150 pc is by no means the limit of the spectroscopic methods. On the contrary, we expect to obtain *Kiel diagrams* as accurate as the one in the upper panel of Fig. 26 for the nearest globular clusters within the next few years. For stars of the same age and chemical abundance the corresponding main-sequence, turnoff and sub-giant region will necessarily be much better defined compared to our heterogeneous field star sample. The basic advantages of diagrams of this kind are then immediately at hand: no color-T_{eff} transformations, no interstellar reddening uncertainties, no distance moduli uncertainties, no bolometric corrections. The scope of this physical diagram must indeed be dramatic.

References

Abt, H.A., Levy, S.G., 1976, ApJS 30, 273
Alonso, A., Arribas, S., Martínez-Roger, C., 1995, A&A 297, 197
Alonso, A., Arribas, S., Martínez-Roger, C., 1996, A&AS 117, 227

Balachandran, S., 1990, ApJ 354, 310

Baliunas, S.L., et al., 1983, ApJ 275, 752

Baliunas, S.L., et al., 1985, ApJ 294, 310

Beavers, W.I., Eitter, J.J., 1986, ApJS 62, 147

Bergbusch, P.A., VandenBerg, D.A., 1992, ApJS 81, 163

Butler, R.P., et al., 1997, ApJ 474, L115

Carney, B.W., 1979, ApJ 233, 211

Carney, B.W., et al., 1994, AJ 107, 2240

Chiappini, C., Matteucci, F., Gratton, R., 1997, ApJ 477, 765

Cochran, W.D., Hatzes, A.P., 1994, BAAS 26, 868

Code, A.D., et al., 1976, ApJ 203, 417

Deeming, T.J., 1960, MNRAS 121, 52

Duquennoy, A., Mayor, M., 1991, A&A 248, 485

Edmunds, M.G., et al., 1991, MNRAS 251, 33P

Edvardsson, B., et al., 1993, A&A 275, 101

Eggen, O.J., 1965, AJ 70, 19

Gehren, T., 1975, *LTE-Sternatmosphärenmodelle*, Kiel

Ghez, A.M., et al., 1995, AJ 110, 753

Gratton, R., Carretta, E., 1996, ASP Conf. Ser. 92, 371

Gratton, R.G., Carretta, E., Castelli, F., 1996, A&A 314, 191

Gratton, R., et al., 1996, ASP Conf. Ser. 92, 307

Gray, D.F., 1977, ApJ 218, 530

Gray, D.F., 1984, ApJ 281, 719

Gray, D.F., 1992, *The observation and analysis of stellar photospheres*, Cambridge Univ. Press

Grevesse, N., Noels, A., Sauval, A.J., 1996, ASP Conf. Ser. 99, 117

Halliwell, M., 1981, ApJS 47, 243

Hearnshaw, J.B., 1972, MmRAS 77, 55

Hearnshaw, J.B., 1974a, A&A 34, 263

Hearnshaw, J.B., 1974b, A&A 36, 191

Hearnshaw, J.B., 1976, A&A 51, 71

Heintz, W.D., 1993, AJ 105, 1188

Heintz, W.D., 1996, ApJS 105, 475

Holweger, H., Müller, E.A., 1974, Solar Phys. 39, 19

Jahreiß, H., Fuchs, B., Wielen, R., 1997, ESA SP-402, p.587

Jones, R.B., 1931, Lick Obs. Bull. 15, 120

Kamper, K.W., Beardsley, W.R., 1986, AJ 91, 419

King, J.R., 1997, AJ 113, 2302

Kurucz, R.L., 1992, Rev. Mex. Astron. Astrofis. 23, 45

Kurucz, R.L., Furenlid, I., Brault, J., Testerman, L., 1984, *Solar Flux Atlas from 296 to 1300 nm*, KPNO, Tucson

Lennon, D.J., et al., 1996, ApJ 471, L23

Lindegren, L., 1997, ESA SP-402, p.13

Majewski, S.R., Phelps, R.L., Rich, R.M., 1997, ASP Conf. Ser. 112, 1

Mermilliod, J.-C., Mermilliod, M., Hauck, B., 1997, A&AS 124, 349

Morbey, C.L., Griffin, R.F., 1987, ApJ 317, 343

Murdoch, K.A., Hearnshaw, J.B., Clark, M., 1993, ApJ 413, 349

Ng, Y.K., Bertelli, G., 1998, A&A 329, 943

Nissen, P.E., 1995, IAU Symp. 164, 109

Nissen, P.E., Schuster, W.J., 1997, A&A 326, 751

Nissen, P.E., Høg, E., Schuster, W.J., 1997, ESA SP-402, p.225

Noyes, R.W., et al., 1984, ApJ 279, 763

Perryman, M.A.C., Lindegren, L., Turon, C., 1997, ESA SP-402, p.743

Pfeiffer, M.J., et al., 1998, A&AS 130, 381

Pont, F., et al., 1998, A&A 329, 87

Quinn, P.J., Hernquist, L., Fullagar, D.P., 1993, ApJ 403, 74

Rocha-Pinto, H.J., Maciel, W.J., 1996, MNRAS 279, 447

Schmidt, E.G., 1972, ApJ 174, 595

Schuster, W.J., Nissen, P.E., 1988, A&AS 73, 225

Schuster, W.J., Parrao, L., Contreras Martínez, M.E., 1993, A&AS 97, 951

Soderblom, D.R., Mayor, M, 1993, AJ 105, 226

Steffen, M., 1985, A&AS 59, 403

Strassmeier, K.G., et al., 1990, ApJS 72, 191

VandenBerg, D.A., Bolte, M., Stetson, P.B., 1996, ARA&A 34, 461

Wheeler, J.C., Sneden, C., Truran, J.W.,Jr., 1989, ARA&A 27, 279

Wyse, R.F.G., Gilmore, G., 1995, AJ 110, 2771